Correspondence between discrete and continuous models of excitable media: Trigger waves

Y. B. Chernyak,* A. B. Feldman, and R. J. Cohen
Division of Health Sciences and Technology, Harvard University–Massachusetts Institute of Technology, Cambridge, Massachusetts
(Received 27 August 1996)

We present a theoretical framework for relating continuous partial differential equation (PDE) models of excitable media to discrete cellular automata (CA) models on a randomized lattice. These relations establish a quantitative link between the CA model and the specific physical system under study. We derive expressions for the CA model's plane wave speed, critical curvature, and effective diffusion constant in terms of the model's internal parameters (the interaction radius, excitation threshold, and time step). We then equate these expressions to the corresponding quantities obtained from solution of the PDEs (for a fixed excitability). This yields a set of coupled equations with a unique solution for the required CA parameter values. Here we restrict our analysis to ''trigger'' wave solutions obtained in the limiting case of a two-dimensional excitable medium with no recovery processes. We tested the correspondence between our CA model and two PDE models (the FitzHugh-Nagumo medium and a medium with a ''sawtooth'' nonlinear reaction source) and found good agreement with the numerical solutions of the PDEs. Our results suggest that the behavior of trigger waves is actually controlled by a small number of parameters. [S1063-651X(97)13702-3]

PACS number(s): 87.22.−q, 82.20.Wt, 82.40.Ck, 02.70.−c

I. INTRODUCTION

Excitable media are spatially extended systems that support solitary waves that propagate unattenuated over long distances. Common examples of excitable media are nerve and muscle tissue in living organisms [1,2], chemical reaction systems [3–6], solid-state electronic systems [7], ecological models [8], and the aggregation of slime molds [9]. These nonequilibrium media have been studied theoretically using nonlinear partial differential equation (PDE) models (reaction-diffusion equations) and also discrete state cellular automata (CA) models. Both of these representations qualitatively reproduce many features of real excitable media. In PDE models, the model parameters are usually identified with physical parameters of the medium, so the relation to real physical systems is well established. For typical CA models, such a connection does not exist, and a physically self-consistent procedure for linking CA models to real physical media has so far remained elusive (but see the recent probabilistic automaton approach of Weimar and Boon [10]). The establishment of such a link is highly desirable, since CA simulations are more efficient computationally than numerical solution of the PDEs, and in many cases may provide a more physically realistic representation of the medium. Further, the simplicity of CA models can yield deeper insights into the underlying processes that determine the behavior of the system. The quantitative link can thus lead to the development of reliable CA models that capture only the relevant features of wave propagation in specific media. These models may be used to perform systematic studies of large statistical ensembles of spatially inhomogeneous or disordered media and media that additionally possess high sensitivity to initial conditions. Such studies are essential for understanding arrhythmia development in the diseased heart.

The goal of this paper is to establish a framework for linking CA models to real physical media. Our strategy is to exploit the fact that the PDE models for specific media are expressed in terms of the physical parameters of the system, so their solutions can be used as an intermediate link to connect the CA model to the physical world. This strategy is fundamentally different from that of Weimar and Boon [10], who incorporate the explicit reaction kinetics of the PDEs into the CA rules. Instead, we introduce a procedure for matching specific features of the traveling wave *solutions* of the PDE model and the CA model in a physically self-consistent way. We consider some basic solutions, such as plane waves and circular waves, and match the values of the parameters of these solutions (e.g., the wave speed, the critical curvature) in both representations of the medium. The matching conditions constitute the quantitative link between the CA model and the specific physical system under study (though for some media the values of many PDE model parameters are not precisely known). A similar strategy was recently employed with some success by several groups [11–13]. Our approach is distinguished by its rigorous and systematic treatment of the behavior at small and large wavefront curvatures. The latter plays an important role in pattern formation and vortex wave dynamics. Here, we use a simple CA model and restrict our analysis to ''trigger wave'' solutions arising in the limiting case of a medium without a recovery process. We must emphasize that this analysis is the required first step in the development of more complex CA models linked quantitatively to the recovery processes of the medium.

To illustrate our basic approach, we consider the propagation of the plane trigger wave shown in Fig. 1. In this CA model, each automaton (or element) possesses two states, resting and excited, and switches between them according to a specific transition rule. The figure depicts an arbitrary rest-

*Author to whom correspondence should be addressed. Present address: Division of Health Sciences and Technology, Office E25-330, Massachusetts Institute of Technology, Cambridge, MA 02139. FAX: (617) 253-3019. Electronic address: yurich@atrium.mit.edu

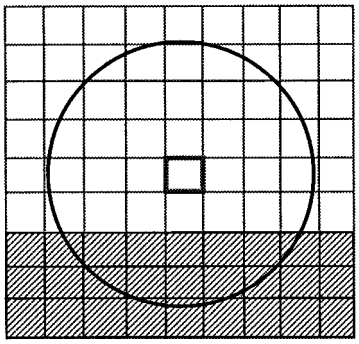

FIG. 1. Excitation rule for a simple cellular automata model of an excitable medium. The cell at the center of the circle (outlined in bold) switches from the resting to the excited state at the next time step when the number of excited elements (shaded) inside the circle equals or exceeds the central element's threshold value. The model parameters are the circle radius R, the excitation threshold K, and the time step Δt.

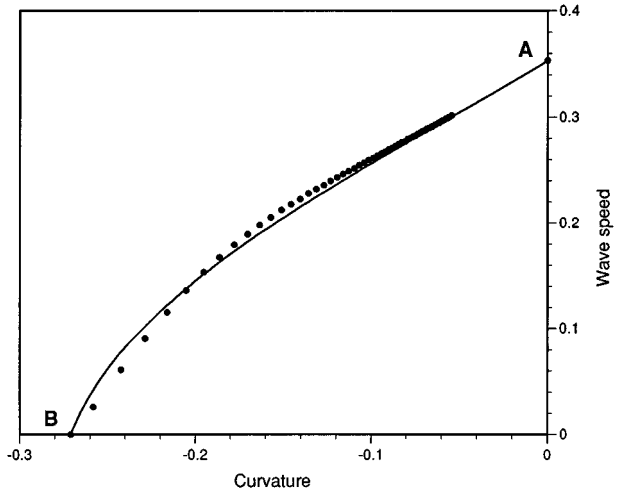

FIG. 2. Wave speed C vs wave-front curvature κ for convex wave fronts in an isotropic two-dimensional excitable medium. The points were obtained via numerical solution of the FitzHugh-Nagumo PDE model [14,15] in the limit of no recovery process. The solid line is the corresponding theoretical relation for our CA model obtained using the required values of R, K, and Δt. The points labeled A and B are the points used to match the PDE and CA representations of the medium. The third matching criterion was the slope at $\kappa=0$, which for trigger waves is numerically equal to the diffusion coefficient D of the propagating species. (All quantities are computed in dimensionless units for a specific normalization of the PDEs).

ing element (the central element shown in bold) and the overlap of its circular interaction neighborhood with the oncoming plane wave of excited elements (shaded). The transition rule states that the resting element at the center switches to the excited state at the next time step when the number of excited elements inside the neighborhood exceeds a threshold value. The model's parameters are the circle radius R, the excitation threshold K, and the time step Δt. For a suitably randomized lattice, the simple transition rule allows us to derive the expressions for the speed of trigger wave fronts with arbitrary curvatures in terms of these three parameters. As we shall show, this simple three parameter CA model reproduces the major features of trigger wave propagation in two-dimensional isotropic media.

Figure 2 shows the wave speed C versus the local wave-front curvature κ for convex trigger waves for both the CA and PDE representations of a specific medium. In two-dimensional media, the behavior of trigger waves is determined almost entirely by this curve, and it therefore captures the major features of trigger wave dynamics. In the figure, the dots represent the points obtained via numerical solution of the FitzHugh-Nagumo PDE model [14,15] (see Sec. V A) and the solid line plots the corresponding relation for the CA model obtained using our matching procedure. The three important features of the plot are the plane wave speed C_0 (point A), the slope D at point A, and the critical curvature κ_{cr} corresponding to vanishing wave speed (point B). The matching between the PDE and CA solutions requires that these three quantities coincide in both representations of the medium. For specific PDEs (with fixed parameter values), this generates three equations for the three unknown values of R, K, and Δt. The physical matching requirements determine unique values for each CA model parameter, thus there is no freedom to vary these values independently. The correspondence between the CA and PDE representations of the medium is quite remarkable.

A. Background

An excitable medium may be viewed as a continuum of diffusively coupled elements, each possessing a stable resting state and at least one metastable excited state. An element in the resting state can switch to the excited state if the local value of the diffusing quantity (the concentration of a chemical reactant or the membrane potential in neuromuscular tissue) exceeds the element's excitation threshold. Diffusion from excited to neighboring resting elements causes the resting elements to exceed threshold and excite, thus spreading an excitation wave spatially. Locally, the wave is characterized by a rapid transition phase during which the element switches to the excited state, followed by a recovery phase during which the element gradually recovers its excitability and slowly returns to rest. The combination of diffusive coupling and temporal variations in excitability gives rise to a variety of traveling wave patterns.

Excitable media are described mathematically by coupled nonlinear PDEs that are difficult to study analytically. The structure of the solitary wave solutions can usually be found using the singular perturbation approach [16,17], which exploits the fact that the excitation and recovery processes occur on very different time scales and therefore the ratio ε of the excitation to recovery time scale can be used as a good smallness parameter. In the limit of small ε, the wave front becomes a moving boundary layer separating the resting and excited regions. When $\varepsilon \to 0$ and the wave-front curvature tends to zero, the motion of these boundaries obeys certain equations of motion that constitute the basis for a kinematic approximation [18–22]. The kinematic approach is philosophically similar to the use of the eikonal approximation in electromagnetic theory, which is a first order PDE describing the domain of geometrical optics. The classical Hamilton-Jacobi equation plays a similar role for the Schrödinger wave equation in quantum theory. If the width of the wave front is

much smaller than the wave front's radius of curvature, then the wave-front position is well defined and the kinematic approach is expected to adequately represent the behavior of the system. Just as the validity of geometrical optics breaks down on the distance scale of a wavelength, the kinematical theories of excitable media must break down when the wave-front curvature radius is on the order of the wave-front thickness [23]. This is because when the system undergoes such abrupt spatial variations, the diffusion processes dominate and the profile of the wave is not even approximately constant in time, thus the notion of a wave front is ill defined. Despite their limitations, both kinematic and perturbation methods have made important contributions to the understanding of pattern formation in excitable media (see Meron [18] for an excellent review).

Clearly, the most straightforward and reliable method for studying complex wave patterns is direct numerical solution of the PDEs [24–26]. Due to the complexity of these equations, such solutions usually consume enormous computational resources and it is generally impractical to perform systematic studies including a statistical ensemble of parameters and initial conditions. Similar considerations apply to lattice gas automata (LGA) [27], which are based on the microscopic reactive particle dynamics and are even more computationally intensive than the PDEs. LGA models are useful for description of phenomena on a scale between the molecular and the macroscopic (the scale at which the reaction-diffusion PDEs represent an appropriate ''mean field'' approximation [27]). It is important to note that since the reaction-diffusion PDEs are coupled and nonlinear, it is difficult to develop intuition for the physical mechanisms that control the macroscopic behavior of the system. The above facts have shifted considerable attention to more efficient CA models of excitable media [11,13,28–32]. Qualitatively, these models demonstrate remarkably similar behavior to PDE solutions and experiments, but there remains no physically consistent method for determining the correct CA parameter values for specific media. In the remainder of this paper, we present a theoretical framework that allows us to calculate these parameter values in the $\varepsilon \to 0$ limit. We restrict ourselves to the class of CA models that do not explicitly incorporate the reaction kinetics of the PDEs.

B. Roadmap

This paper consists of five sections. In Sec. II, we consider the continuous PDE representation of an excitable medium. We analyze the trigger wave solutions and review the technique for finding the plane wave speed. We also introduce a suitable definition for the critical curvature and show how to calculate it from the PDEs. In Sec. III, we describe our CA model in detail and derive the analytic expression for the plane wave speed in terms of the CA model parameters. In the following section, we consider the effects of curvature on the propagation speed, which allows us to find the expressions for the effective diffusion constant and for the critical curvature. In Secs. III and IV, we also compare the results of our theoretical calculations with CA model simulations. Finally, in Sec. V we establish the correspondence between the continuous PDE and discrete CA representations. We consider two specific PDE models with fixed parameter values: the FitzHugh-Nagumo medium and a medium described by a reaction-diffusion equation with a ''sawtooth'' nonlinear source. We conclude the paper with a brief discussion of CA modeling of spatially inhomogeneous media and with a comparison of this work to other recent approaches.

II. CONTINUOUS MODELS OF EXCITABLE MEDIA

A minimum model of an excitable medium is described by two variables that obey a set of the reaction-diffusion equations [18], which can be written in the form

$$\frac{\partial u}{\partial t} = D\nabla^2 u + \frac{f(u,v)}{\tau_u}, \tag{1}$$

$$\frac{\partial v}{\partial t} = \frac{g(u,v)}{\tau_v}, \tag{2}$$

where ∇^2 is the Laplacian operator in spatial coordinates (x,y,z), t is time, u represents the ''concentration'' of the diffusively propagating species, v is a recovery variable that controls the local recovery of excitability, D is the diffusion coefficient of u, and τ_u and τ_v are the time scales associated with the evolution of u and v, respectively. The ratio $\varepsilon = \tau_u/\tau_v$ typically satisfies $\varepsilon \ll 1$. The exact interpretation of u and v depends on the particular system under study. In neuromuscular tissue, u represents the transmembrane potential and the time scale τ_u is equal to the maximum membrane conductivity for the ''fast'' ionic current divided by the specific membrane capacitance. The quantity τ_v may be interpreted as this same ratio for a ''slow'' repolarizing current v. The function $-f(u,v)$ is the rescaled current-voltage characteristic of the membrane. In neuromuscular tissue, the diffusion constant D depends only on the passive properties of the cells: the intracellular conductivity, the specific membrane capacitance, and the surface area to volume ratio. In multidimensional tissues, D is a tensor $\tilde{D}$, and thus the second order derivative term in Eq. (1) should be written $\nabla\cdot(\tilde{D}\nabla u)$. For now, we restrict our analysis to the special case of a homogeneous and isotropic medium (D is a scalar constant). In dimensionless form, Eqs. (1) and (2) may be written as

$$\frac{\partial u}{\partial t'} = \nabla'^2 u + f(u,v), \tag{3}$$

$$\frac{\partial v}{\partial t'} = \varepsilon g(u,v), \tag{4}$$

where $t' = t/\tau_u$, and the space coordinates x_i' are given by $x_i' = x_i/\sqrt{D\tau_u}$. In subsequent analysis, all the primes of space and time coordinates are omitted unless explicitly stated otherwise.

Equations (3) and (4) describe a continuous system that consists of a continuum of diffusively connected identical dynamical elements each described by a set of ordinary differential equations $\dot{u} = f(u,v)$ and $\dot{v} = g(u,v)$. The functions $f(u,v)$ and $g(u,v)$ in Eqs. (3) and (4) describe the local nonlinear kinetics of the system's elements. A typical phase diagram for the local kinetics is shown in Fig. 3. The u nullcline $f(u,v)=0$ generally has two stable, monotonically

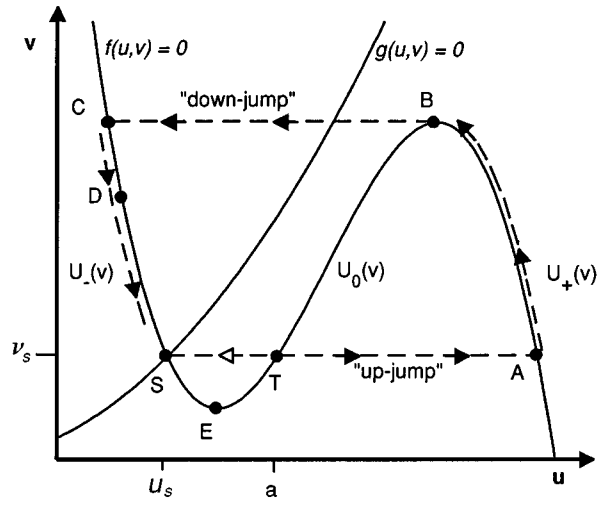

FIG. 3. Typical phase diagram for an excitable medium described by Eqs. (3) and (4). The intersection point S of the nullclines $f(u,v)=0$ and $g(u,v)=0$ is the unique resting state of the system. The resting state is ''excitable,'' meaning that for small perturbations of u the system immediately returns to S, but large perturbations beyond the threshold value a initiate the long excursion in phase space indicated by the dashed line. The horizontal segment TA (''up-jump'') represents the fast transition of u from the resting to the excited state. While in the excited state AB, v slowly increases, which eventually results in the triggering of the rapid reverse transition BC (''down-jump'') from the excited to the refractory state. This state is characterized by the slow decrease of v and the gradual recovery of excitability of u as the system returns to S. If the system is sufficiently recovered (beyond the point D on the trajectory), a new excitation may be triggered provided the perturbation δu shifts u beyond the branch $U_0(v)$ (segment EB). In the limit $\varepsilon\to 0$, the system only supports the transition TA, since the time scale of evolution of v is infinite. The system thus remains indefinitely at point A and never returns to S.

decreasing solution branches $u=U_+(v)$, $u=U_-(v)$, and an unstable, monotonically increasing branch $u=U_0(v)$ [33]. The function $g(u,v)=0$ is assumed to be a monotonically increasing function of u, which intersects the curve $f(u,v)=0$ at a single point S. The point S is stable with respect to small perturbations and corresponds to the ''resting'' state of the system. When u is perturbed beyond the threshold value a, u increases abruptly (excites), which initiates the long excursion ($TABCD$) in phase space shown in Fig. 3 before finally returning to S. In a spatially extended system, suprathreshold perturbations are provided by diffusion of u from excited regions, which spreads the excitation wave spatially.

Note that the set (3) and (4) constitutes a minimum model of an excitable medium in three respects: first, in the more general case there may be more than one recovery variable, $v_1,v_2,\ldots,v_n$, each controlled by an equation similar to Eq. (4); second, the v-type quantities may also spread diffusively, so in the right hand side of Eq. (4) a diffusion term proportional to $\nabla^2 v$ can be added; and finally, the nonlinear source is assumed to be instantaneously activated (i.e., the time constant of ''turn on'' of the source is zero). In neuromuscular tissue, the variable u is the only diffusing quantity and is identified with the local transmembrane potential, which is appropriately averaged over a physically infinitesimal region [34], i.e., over a region including many cells, but still small compared with the size of the system. On the other hand, in these tissues there are a variety of processes (described by v-type quantities) responsible for termination of excitation and restoration of the initial state, such as the inactivation (''turn off'') of the sodium current and the repolarization by the potassium current. The description of these processes evidently requires more than one v variable, so direct interpretation of the second equation (4) in terms of electrophysiological quantities is not always possible (but see Refs. [35–37]).

Solitary wave solutions to the system of equations (3) and (4), valid for small ε may be analyzed using a perturbation approach [16]. According to Eq. (4), when $\varepsilon\ll 1$ the variable v evolves slowly, on a characteristic time scale $1/\varepsilon$, and remains approximately constant when u is changing rapidly in the wave-front region. In the limit $\varepsilon\to 0$, we have $\partial v/\partial t=0$, and hence $v=v_s=$const, where v_s is the initial resting v value. One can see that Eq. (3) has constant solutions that satisfy the equation $f(u,v_s)=0$. This equation has two stable solutions $u=U_-(v_s)$ and $u=U_+(v_s)$ corresponding to the resting and excited states, respectively (see Fig. 3). We are interested in a traveling wave solution joining these two stable states, one residing at $+\infty$ (resting) and the other at $-\infty$ (excited). The wave front is therefore *a moving boundary layer* connecting two plateau regions in which $u=U_-(v_s)$ and $u=U_+(v_s)$, respectively. These ''ignition'' or ''trigger'' wave solutions resemble those in bistable media, where elements remain in the excited state indefinitely after firing. For a specific v_s, the profile of the wave front and the (dimensionless) propagation speed $\hat{c}_0$ are found by seeking a traveling wave solution of Eq. (3) of the form of a steadily propagating plane wave $u(\xi)$, where $\xi=x-\hat{c}_0 t$. Substituting $u=u(\xi)$ into Eq. (3) and using Eq. (4) with $\varepsilon=0+$ we arrive at the following nonlinear eigenvalue problem [38]:

$$\frac{d^2u}{d\xi^2}-\hat{c}_0\frac{du}{d\xi}+f(u,v_s)=0, \tag{5}$$

$$\lim_{\xi\to\infty}u(\xi)=U_-(v_s), \qquad \lim_{\xi\to-\infty}u(\xi)=U_+(v_s). \tag{6}$$

The solution of this problem is the profile of the trigger wave $u=u(\xi)$ and the dimensionless propagation speed $\hat{c}_0$ (the eigenvalue). This problem must generally be solved numerically for specific $f(u,v)$ [39], although some classes of exact solutions and semianalytical approaches may also be useful [40–44]. A trigger wave profile obtained numerically for a simple model of ventricular myocardium is shown in Fig. 4.

In dimensional terms, the plane wave speed C_0 is given by $C_0=\hat{c}_0\sqrt{D/\tau_u}$ and is a lumped parameter characterizing each plane wave solution of system (3) and (4). Mathematically this quantity is a functional of $f(u,v_s)$. For each solution of Eqs. (5) and (6), we define the specific length and time scales

$$L_0\equiv\frac{D}{C_0}, \qquad \tau_0\equiv\frac{L_0}{C_0}=\frac{D}{C_0^2}. \tag{7}$$

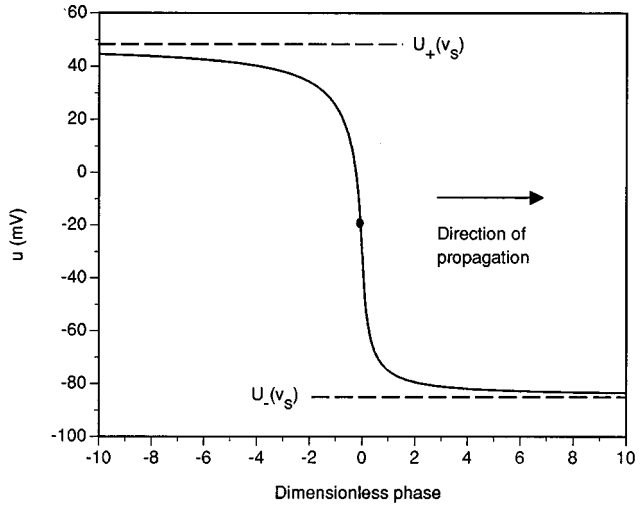

FIG. 4. Trigger wave profile $u(\xi)$ obtained using the fully activated, ''fast'' ionic currents in ventricular myocardium (see Ref. [39] for details). The quantity u represents the transmembrane potential. The origin ξ_0 for the dimensionless phase $\xi=x-\hat{c}_0 t$ was chosen to coincide with the inflection point of $u(\xi)$ ($du/d\xi$=max). This point is indicated by the dot. The wave front $u(\xi)$ is a moving boundary layer separating resting $[u=U_-(v_s)]$ and excited $[u=U_+(v_s)]$ regions. For the model used above, v_s is identically zero.

In the limit $\varepsilon\to 0$, the quantity $\tau_0=\tau_u/\hat{c}_0^2$ is the *only characteristic time* for front formation of the plane wave. To understand this, we first note that if we rescale the source $f(u,v)$ by a factor λ, then the eigenvalue $\hat{c}_0$ must rescale by a factor $\lambda^{1/2}$ [42,43]. Further, note that in Eq. (1) if we scale τ_u by a factor λ, we must also scale $f(u,v)$ by λ in order not to change the magnitude of the source term. Thus $\tau_0=\tau_u/\hat{c}_0^2$ remains invariant with respect to this scaling.

In two dimensions, the eigenvalue problem for wave fronts with curvature κ yields [46,33] the following approximate expression for the dimensional wave speed C:

$$C=C_0+D\kappa. \tag{8}$$

The curvature of the front κ is related to its curvature radius r by $\kappa=\pm 1/r$, where it is implied that $r>0$ and the minus sign corresponds to a convex wave front and the plus sign corresponds to a concave front. Since the outer normal to the front is commonly chosen in the direction of propagation, $\kappa>0$ for a concave front and $\kappa<0$ for a convex front. Equation (8) can be understood from the well known fact that the Laplace operator ∇^2 in the axially symmetric case is given by $\partial^2/\partial r^2+(1/r)\partial/\partial r$. The term with the first derivative is proportional to the curvature $\kappa=1/r$ of the coordinate surface $r=$const, and on substitution into Eq. (3) gives rise to the second term in Eq. (8). This was first observed by Zeldovich in 1944 in his analysis of the stabilizing effect of curvature on flame front propagation [45]. In the limit $\varepsilon\to 0$, expression (8) can also be derived very elegantly from simple geometric considerations for a steadily propagating wave [46].

The accelerating influence of concave fronts and the retarding effect of convex fronts reflects the underlying diffusive mechanism of the spread (note the curvature correction to the plane wave speed is proportional to the diffusion constant D). This idea is illustrated in Fig. 5. Wave fronts with positive curvature (concave) tend to focus the diffusive flux, which reduces the time required to exceed threshold ahead of the front. This increases the propagation speed relative to a plane wave. Conversely, a convex front (negative curvature) defocuses the diffusive flux which retards the progress of the front. According to Eq. (8), the front speed C vanishes at a *critical curvature* $\kappa_{\rm cr}$ of the order of $-C_0/D$. This expression is an estimate of the critical curvature, since at large convex curvatures the front's shape may change appreciably on the time scale of front formation τ_0 (nonsteady propagation). In this case, the speed may depend nonlinearly on the curvature and may also depend on tangential derivatives of u along the front [18].

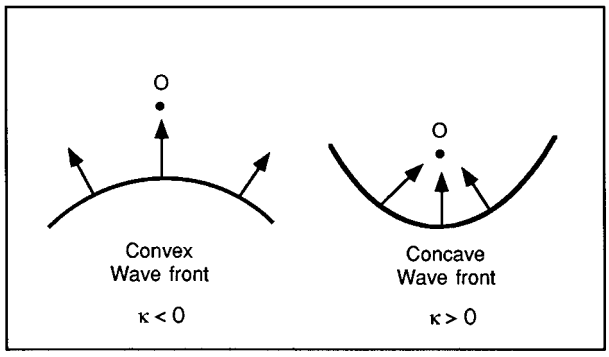

FIG. 5. The focusing (concave) and defocusing (convex) effects of wave-front curvature on excitation. A convex shape tends to reduce the diffusive flux per unit time (current) into point 0 ahead of the wave front, thereby increasing the time required to exceed the excitation threshold at point 0. This reduces the speed of a convex wave relative to a plane wave. Conversely, a concave wave front will tend to increase the current, which results in a faster speed than a plane wave.

For trigger waves, we may obtain a value of $\kappa_{\rm cr}$ from the steady state (zero speed) solution $u_{\rm cr}(\rho)$ of Eqs. (3) and (4), where ρ is the radial coordinate. Setting $\partial u/\partial t=0$ and $\partial v/\partial t=0$ in these equations we have

$$\frac{d^2u_{\rm cr}}{d\rho^2}+\frac{\nu}{\rho}\frac{du_{\rm cr}}{d\rho}+f(u_{\rm cr},v_s)=0, \tag{9}$$

where $\nu=1$ or $\nu=2$ in the two- or three-dimensional case, respectively. The solution of Eq. (9) is subject to the requirement that $u_{\rm cr}(\rho)$ is bounded in the interval $0<\rho<\infty$. It can be shown that this condition results in a monotonically decreasing $u_{\rm cr}(\rho)$ with the derivatives vanishing at both ends of the interval $0<\rho<\infty$ (a cross section through a typical solution for $u_{\rm cr}(\rho)$ is shown in Fig. 19). We use the stationary (zero speed) wave profile $u_{\rm cr}(\rho)$ to define a characteristic radius $\rho_{\rm cr}$. To accomplish this, we first introduce the renormalized derivative

$$p_{\rm cr}(\rho)=-\frac{1}{u_{\rm cr}(0)}\frac{du_{\rm cr}(\rho)}{d\rho}. \tag{10}$$

The monotonicity of $u_{\rm cr}(\rho)$ allows us to consider $p_{\rm cr}(\rho)$ as a probability density function, and $\rho_{\rm cr}$ can be defined as a characteristic measure of this distribution, for example, the mode

(maximum) or first moment. The critical curvature κ_{cr} is then the negative of the inverse of ρ_{cr}:

$$\kappa_{cr} = -\frac{1}{\rho_{cr}}. \tag{11}$$

We note that when ε is nonzero, no such steady-state solution exists and propagation is terminated at a critical nonzero wave speed (see [22] for an analytical estimation of this quantity in the kinematic limit).

For each reaction-diffusion medium described by specific functions $f(u,v)$ and $g(u,v)$, we have shown how to calculate the unique values of the plane wave speed C_0 and critical curvature κ_{cr} for trigger waves. These two quantities are ''lumped'' solution parameters that are functionals of the nonlinear source $f(u,v_s)$. Together with the diffusion constant D, these quantities determine the major features of the plot of the propagation speed versus wave-front curvature (the plot shown in Fig. 2): C_0 is the intercept at $\kappa=0$, D is the slope at $\kappa=0$, and κ_{cr} is the intercept with the abscissa. In the following sections, we describe a discrete CA model and show that its parameters can be defined in such a way that its trigger wave solutions have the same characteristics D, C_0, and κ_{cr} as in the continuous medium.

III. DISCRETE MODELS OF EXCITABLE MEDIA

Since their introduction in 1946 by Wiener and Rosenblueth, discrete CA models have made important contributions to the understanding of wave processes in excitable media [28–31] (see also Ref. [47] for CA approaches in chemical media and Ref. [48] for formal properties of cellular automata). Typical CA models consist of a two- or three-dimensional array of identical elements arranged on a square lattice. Each element represents a square or cube of excitable medium and switches between a finite number of states according to specific state transition rules. The simplest models possess three states: excited, refractory, and resting (excitable), with the interactions between the elements restricted to the nearest neighbors on the lattice. In terms of a diffusive process, the excitation rules can be viewed as reflecting the ''sourcing of the diffusing substance'' by excited elements to their resting neighbors. In ''edge-triggered'' models [49], an excited element switches its resting neighbor into the excited state at the next time step, which spreads the wave spatially. This excitation rule suffers from the drawback that the resulting wave fronts acquire the shape of the lattice elements (square) and propagate at speeds that depend on direction (anisotropy). This scheme also cannot incorporate the effects of wave-front curvature on propagation speed, since an element is only excited by its nearest neighbors and thus does not sense the shape of the oncoming wave front (as reflected by the spatial distribution of excited elements).

CA models of excitable media were made more realistic by the introduction of non-nearest-neighbor interaction rules [32,11]. In these models, elements interact with all neighboring elements inside a region of characteristic size R (e.g., a circle with radius R, or a square with side R). We shall refer to R as the interaction radius and denote it by R_d when expressed in lattice units Δx ($R \equiv R_d \Delta x$). The scheme studied extensively by Markus and Hess [11] is shown in Fig. 6.

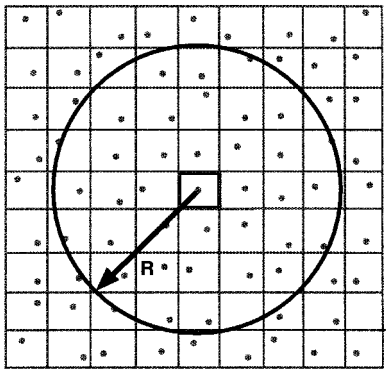

FIG. 6. The lattice randomization scheme of Markus and Hess [11] used in our simple discrete CA model. One seed point is assigned to a random location inside each square element. The neighbors of the central element are determined by locating all elements whose seed points fall inside the circle of radius R centered on the seed point of the central element.

In the figure, each seed point is assigned to a random location inside each element and the central element's neighbors are determined by locating all elements whose seed points fall inside a circle of radius R emanating from the seed point of the central element. The central element switches from the resting to the excited state when the number of excited neighbors equals or exceeds the threshold value K. This interaction occurs in one model time step Δt. For R_d sufficiently large, this interaction rule produces circular wave fronts (on the average), which is essential for modeling continuous isotropic media [50]. We will later show that this property permits us to compute the propagation speed analytically as a function of R, K, and Δt.

In the Markus and Hess model, the effects of wave-front curvature on propagation speed are incorporated automatically (at least qualitatively) because the number of excited neighbors always depends on the local shape of the approaching wave front. Just as in continuous media (Fig. 5), a concave wave front increases the propagation speed relative to a plane wave, since the curvature tends to increase the number of excited (''sourcing'') elements inside R, thus reducing the time required to reach the threshold value K at the center. Conversely, convex wave fronts tend to reduce the number of excited elements, which therefore decreases the wave speed compared to a plane wave. The ability of the model with given R to resolve different values of the curvature depends on the spatial discretization R_d.

A. CA model for trigger waves

In this section, we describe a simple CA model of a two-dimensional excitable medium based on the Markus and Hess scheme (Fig. 6). This model shall only incorporate the minimum necessary features for simulating trigger waves in isotropic media. We therefore omit all quantities related to the recovery processes of the medium, such as the refractory period and the recovery curve (the dependence of the plane wave speed on recovery time). In our model, each element represents a small square region of excitable medium with side Δx. To each model element we assign a seed point at a random location inside its square and three internal *vari-*

ables: a phase or ''autochrone'' T (the time since the previous excitation), an interaction radius R, and an excitation threshold K. The element's neighbors are determined from the interaction radius R as shown in Fig. 6. Note that the randomization of the lattice permits us to treat R as a continuous-valued quantity. Each element is also assigned one internal *parameter*: the exciting state duration T_E, which is the number of time steps that an element is an effective ''source'' to its neighbors. Note that this parameter can be treated as independent of the recovery parameters. For example, in neuromuscular tissue, we may identify T_E with the inactivation time of the fast sodium current. The state U of an element can assume two values, u_R, or u_E, which correspond to the resting and excited states, respectively.

The evolution of the elements' states occurs in time steps Δt and the autochrone T is a dimensionless quantity expressed in Δt units. We shall mark this discrete time as a superscript, so the state transitions of element k from time step n to $n+1$ are governed by its autochrone value T_k^n, its current state U_k^n, and the total source strength supplied by its neighbors Q_k^n defined as

$$Q_k^n = \sum_{\text{neighbors}} w_{kj} S_j , \tag{12}$$

where the index j runs over all elements in the neighborhood R of element k. The coefficients w_{kj} represent the local contribution of element j to the excitation of element k ($0 \leqslant w_{kj} \leqslant 1$), while S_j represent the intensities of the sources:

$$S_j = \begin{cases} S & \text{if } 0 < T_j \leqslant T_{Ej} \\ 0 & \text{otherwise.} \end{cases} \tag{13}$$

Note that w_{kj} may be viewed as reflecting the fraction of the diffusing substance ''sinked'' by element k in one time step Δt from a source at j, while the intensities S_j represent the intrinsic magnitudes of the sources. The distribution w_{kj} is analogous to the ''mask'' introduced by Weimar *et al.* [51] and the element weight function utilized by Fast and Efimov [52]. The state transitions for element k with excitation threshold K_k obey the following rules:

$$U_k^{n+1} = \begin{cases} u_E & \text{if } U_k^n = u_R \text{ and } Q_k^n \geqslant K_k \\ U_k^n & \text{otherwise;} \end{cases} \tag{14}$$

$$T_k^{n+1} = \begin{cases} 0 & \text{if } U_k^{n+1} = u_R \\ T_k^n + 1 & \text{otherwise.} \end{cases} \tag{15}$$

In the CA model, the trigger wave front is represented by a moving spatial discontinuity in the field of U values. In subsequent analysis, we should be mindful that this sharp boundary is artificial, since the interaction actually occurs over a length scale R. Phenomena observed on length scales smaller than R should generally be disregarded (we will later see that R is related to the wave-front spatial scale L_0 of the plane wave PDE solution). Finally, we note that we must be careful to distinguish between the model's spatial resolution R and the spatial discretization $R_d = R/\Delta x$, which controls the statistical averaging of the source strength Q and the resolution of the wave-front shape inside R.

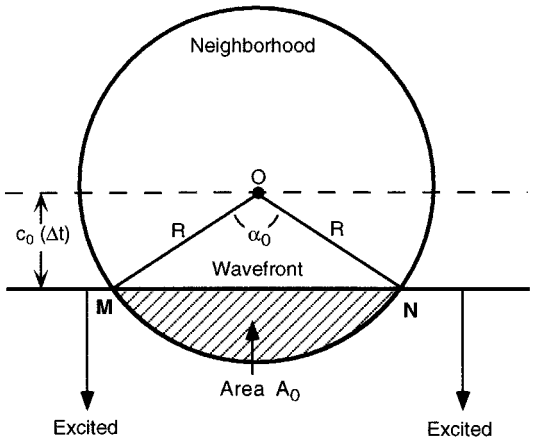

FIG. 7. Geometry for calculating the plane wave speed in the CA model. The underlying square grid (omitted for clarity) is shown in Fig. 6 and has an internode spacing Δx. We consider the marginal case where the element at point O switches to the excited state when the number of its excited neighbors $A_0/\Delta x^2$ is equal to its threshold value K. The wave front MN reaches the point O at the next time step and shifts by the distance $c_0 \Delta t$.

In the sections that follow, we derive explicit expressions for the plane wave speed, critical curvature, and effective diffusion constant for trigger waves in terms of the three parameters R, K, and Δt. The trigger wave solutions are obtained in the limit $T_E \to \infty$, which is analogous to the limit $\varepsilon \to 0$ of the PDEs, since in both cases excited elements source to neighboring elements indefinitely. For the remainder of this paper, we shall use a *minimum* version of the CA model with $w_{ki} \equiv 1$ (a ''flat'' distribution) and all source intensities $S=1$. For this realization of the model, the local source strength Q is always identical to the number of excited neighbors.

B. Plane wave propagation speed

The dependence of the plane wave speed c_0 on the threshold value K can be analyzed analytically for practically any neighborhood shape. Here we consider the circular interaction region with radius $R = R_d \Delta x$ (an anisotropic medium can be described using an elliptical neighborhood). Figure 7 displays the excitation of an arbitrary element located at point O by an oncoming plane wave with wave front MN. Since we have restricted our analysis to $T_E = \infty$, the ''sourcing'' region always extends beyond the edge of the interaction circle (the wave thickness $c_0 T_E$ is infinite for arbitrarily small c_0). According to Eqs. (12)–(15) and Fig. 7, the central element at point O switches to the excited state at the next time step (Δt) and the wave front shifts by the distance $c_0 \Delta t = R \cos(\alpha_0/2)$ when the number of excited neighbors Q inside the circle reaches the threshold value K. Since the lattice is randomized, the number of excited neighbors is on the average $Q = A_0/\Delta x^2$, where A_0 is the area of the shaded portion of the circular neighborhood shown in Fig. 7. The condition for the elements on and behind the planar front to excite point O at the next time step is $Q = K$. Since $A_0 = R^2(\alpha_0 - \sin \alpha_0)/2$, we obtain the following expression for the plane wave speed c_0:

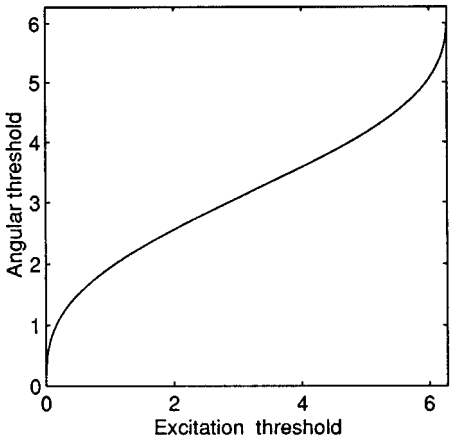

FIG. 8. The angular threshold α_0 vs the dimensionless excitation threshold $\hat{k}=2K/R_d^2$. The function $\alpha_0(\hat{k})$ is universal and is independent of any parameters. We use α_0 as a measure of excitability: high excitabilities correspond to small α_0 (low excitation thresholds $\hat{k}$) while low excitabilities correspond to large α_0 (high excitation thresholds $\hat{k}$).

$$c_0=\frac{R}{\Delta t}\cos\frac{\alpha_0}{2}\equiv R_d\frac{\Delta x}{\Delta t}\cos\frac{\alpha_0}{2}, \tag{16}$$

where α_0 is the solution of the transcendental equation

$$G_0(\alpha_0)\equiv\alpha_0-\sin\alpha_0=\hat{k}\quad\left(\hat{k}\equiv\frac{2K\Delta x^2}{R^2}=\frac{2K}{R_d^2}\right). \tag{17}$$

The function $G_0(\alpha_0)$ defined in Eq. (17) is a monotonically increasing function in the interval $0<\alpha<2\pi$ [its derivative, $G'(\alpha_0)=1-\cos\alpha_0>0$] and varies from $G_0(0)=0$ to $G_0(2\pi)=2\pi$, so it has an inverse function $G_0^{-1}(\hat{k})\equiv\alpha_0(\hat{k})$ in this interval (it actually exists on the whole real axis). Note that when $\alpha_0\ll 1$, $G_0(\alpha_0)\sim\alpha_0^3/6$ and therefore $\alpha_0(\hat{k})\sim\sqrt[3]{6\hat{k}}$ for $6\hat{k}\ll 1$. The function $G_0(\alpha_0)$ is universal, independent of any parameters, and therefore, its inverse function $\alpha_0(\hat{k})$ shown in Fig. 8 is also a universal function independent of any parameters. This fact allows us to use α_0 *itself as a measure of the excitability*. When $\alpha_0\sim 0$ the medium is highly excitable, and when $\alpha_0\sim\pi$ the medium is the least excitable. Note that as discussed in the next subsection, the case $\pi\leqslant\alpha_0<2\pi$ corresponds to such a low excitability that only concave wave fronts can propagate. We shall refer to α_0 as the *angular threshold*. It is interesting that an expression similar to Eq. (16) appeared in a different ''scaling'' relation for the plane wave speed found by Ito [13] using a different modeling approach.

To check relations (16) and (17), we performed simulations of plane waves on a two-dimensional rectangular lattice with periodic boundary conditions in one direction (a cylinder). Each element in the lattice was assigned an identical interaction radius R (R_d in lattice units) and threshold value K. Plane waves were initiated by exciting a band of elements at one end of the cylinder (the width of the band was always wider than R_d units). The propagation speed of the plane waves was computed by tracking the average position (averaged over the seed point locations) of the wave-front edge (the boundary between excited and resting elements). The plane wave speed versus dimensionless threshold $\hat{k}$ for two different spatial discretizations $R_d=R/\Delta x$ is shown in Fig. 9. The curves are the theoretical values obtained using Eqs. (16) and (17). The error bars are the standard deviations of the measured plane wave speeds and represent the statistical fluctuations induced by the lattice randomization. The magnitude of this ''noise'' is approximately independent of c_0, so it becomes progressively more important as $c_0\to 0$. These fluctuations can result in spurious block (termination of the forward progress of the wave) when the shift of the front δ in one time step $\delta\equiv c_0\Delta t$ becomes $\sim\Delta x$, since the success of a wave-front shift on this length scale depends on the specific seed point locations. Arbitrarily small wave speeds can only be simulated reliably in the limit $R_d\to\infty$, $\Delta x\to 0$ when R is held fixed.

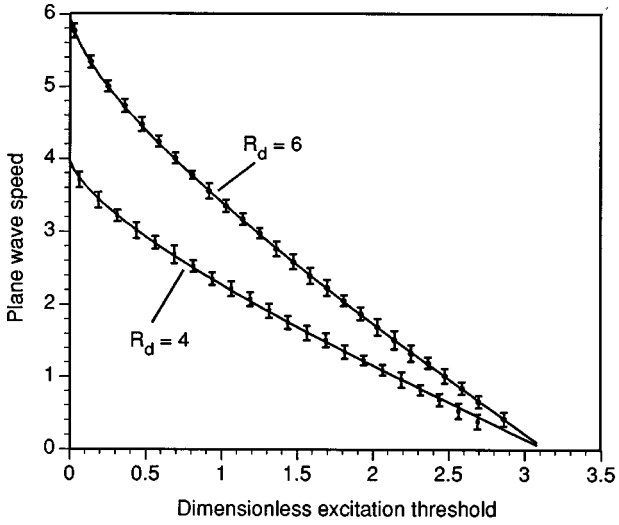

FIG. 9. Measured plane wave speed $c\Delta t/\Delta x$ vs excitation threshold $\hat{k}$ for two different spatial discretizations R_d. The theoretical curves are computed using Eqs. (16) and (17). The wave speeds were obtained by assigning a single threshold K to each element in the lattice and measuring the shift of the wave front δ (averaged over the internal seed point positions) after each successive time step Δt. The points represent the average of δ over 25 time steps and the error bars are the standard deviations.

IV. EFFECTS OF WAVE-FRONT CURVATURE

Similar to the plane wave case, the propagation speed for curved wave fronts can be found from the fact that the average number of the excited elements within the interaction region is proportional to the area of the portion of the interaction region covered by the oncoming wave. It is convenient to define a dimensionless, rescaled curvature $\eta\equiv R\kappa\equiv\pm R/r$. Concave and convex wave fronts correspond to $\eta>0$ and $\eta<0$, respectively, while $\eta=0$ (infinite curvature radius) corresponds to a plane wave. We shall first consider propagation of wave fronts with small to moderate curvature and then we shall study the domain of validity of the obtained equations and the effects at its boundary. We then obtain the expression for the critical curvature by considering the case of vanishing propagation speed. Finally, we consider the dependence of the propagation speed on wave front curvature in the limit $|\eta|\to 0$ and arrive at an expression for the effective diffusion constant of the CA medium.

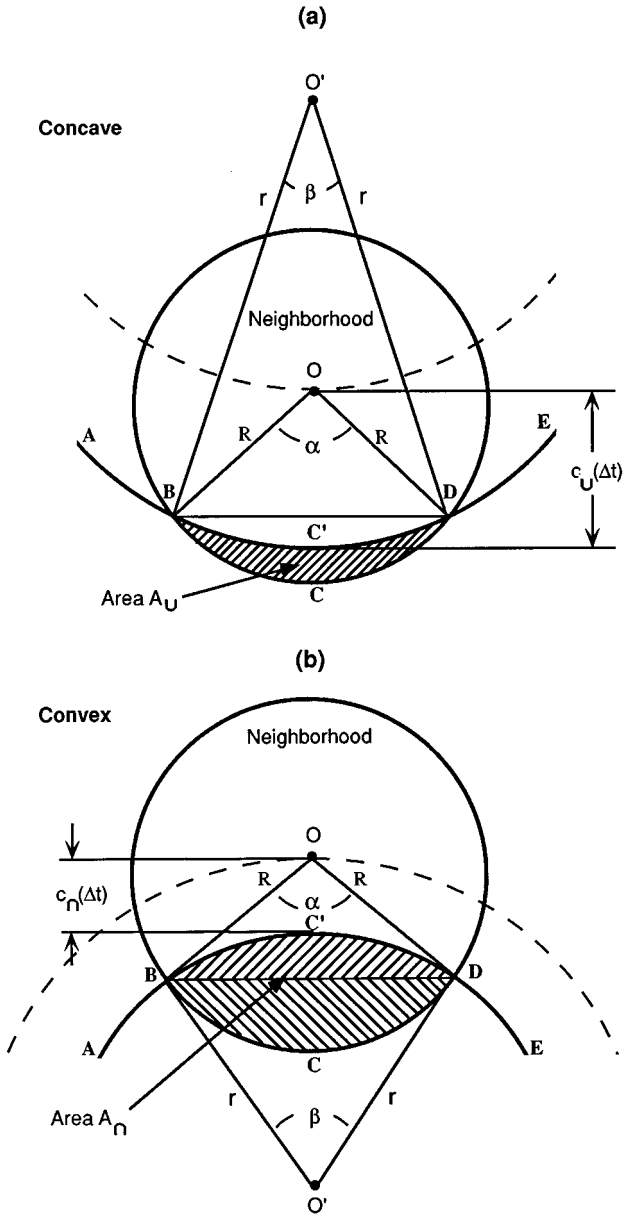

FIG. 10. Geometry for calculating the speed of curved wave fronts in the CA model. The underlying square grid (omitted for clarity) is shown in Fig. 6 and has an internode spacing Δx. The approaching wave front with curvature κ is locally approximated by a circle with radius $r=\pm 1/\kappa$ centered at the point O'. In one time step Δt, the wave front $ABC'DE$ shifts to the point O when the number of excited neighbors (a) $A_\cup/\Delta x^2$ (b) $A_\cap/\Delta x^2$ is equal to the threshold value K (of the element at point O). The wave speeds for concave and convex wave fronts are $c_\cup$ and $c_\cap$, respectively.

A. Wave fronts with small and moderate curvatures

Since the transition from the resting to the excited state occurs over a region with characteristic size R, this value is an effective measure of the wave-front size as well as a measure of the spatial resolution of the discrete model. Thus the curvature range $|\eta|\leqslant 1$ appears to be a natural domain of validity that does not call for a special discussion. We shall start with Figs. 10(a) and 10(b), which show the geometries for calculating the wave-front speeds of concave and convex fronts with moderate curvature $|\eta|\leqslant 1$. In both cases, the figure displays the situation at the moment immediately preceding (by one time step) the excitation of the element at point O. The oncoming wave front $ABC'DE$ is locally approximated by a circle with center O' and radius r. The arc BCD of the interaction circle is subtended by the angle α, which varies generally in the semi-interval $[0,2\pi)$. The arc $BC'D$ of the wave front is subtended by an angle β, which will be considered *positive* if the curvature center O' and the point O lie on the same side of the front, and *negative* otherwise. Such a sign convention allows us to write the equation $R\sin(\alpha/2)=r\sin(|\beta|/2)$ relating the angles α and β in the form

$$\sin\frac{\beta}{2}=\eta\sin\frac{\alpha}{2}, \tag{18}$$

which is valid for both concave and convex wave fronts. A new position of the wave front passing through point O' is shown by the dashed line. As can be seen from Fig. 10, the concave wave front shifts by the distance $|C'O|=c_\cup\Delta t=R\cos(\alpha/2)+[r-r\cos(\beta/2)]$ and the convex wave front shifts by $|C'O|=c_\cap\Delta t=R\cos(\alpha/2)-[r-r\cos(\beta/2)]$. This shift occurs when the number of excited neighbors Q inside the interaction region reaches the threshold value K. The average number of excited neighbors can again be evaluated as $A/\Delta x^2$, where A is the area of the interaction region covered by the oncoming wave [shaded in Figs. 10(a) and 10(b)]. In the concave case, the number of excited neighbors is $A_\cup/\Delta x^2$, where $A_\cup=(R^2/2)(\alpha-\sin\alpha)-(r^2/2)(\beta-\sin\beta)$, and the second term contributes negatively ($\beta>0$). In the case of convex wave fronts, the average number of excited neighbors is $A_\cap/\Delta x^2$, where the area $A_\cap$ is given by the same expression as $A_\cup$, but with the last term contributing positively ($\beta<0$). Using the above expression for the shift $|C'O|$ and equating $Q=A_\cup/\Delta x^2$ and $Q=A_\cap/\Delta x^2$ to the threshold value K we obtain

$$c=\frac{R}{\Delta t}\left\{\cos\frac{\alpha}{2}+\frac{1}{\eta}\left(1-\cos\frac{\beta}{2}\right)\right\}, \tag{19}$$

$$G_0(\alpha)-\frac{1}{\eta^2}G_0(\beta)=\hat{k}\equiv\frac{2K\Delta x^2}{R^2}, \tag{20}$$

where $G_0(\alpha)$ is defined in Eq. (17) and we again introduce the same dimensionless threshold $\hat{k}$ as in Eq. (17). These expressions are valid for both convex and concave wave fronts. Note that G_0 is an odd function and $G_0(\beta)>0$ when $\beta>0$ and $G_0(\beta)<0$ when $\beta<0$. The parameters α and β are related by Eq. (18), and therefore for any fixed η the three relationships (18)–(20) determine a curve on the (k,c) plane. By varying the curvature η, we obtain a family of curves $c=c(\hat{k},\eta)$, which is the object of our further consideration.

Because we have assumed that $|\eta|\leqslant 1$, Eq. (18) can be uniquely solved for β at any α. This is because when $|\eta|\leqslant 1$ or $r\geqslant R$, we always have $|\beta|<\alpha\leqslant\pi$, so Eq. (18) has only one solution $\beta=2\arcsin[\eta\sin(\alpha/2)]$. Substituting this expression into Eqs. (19) and (20) we obtain

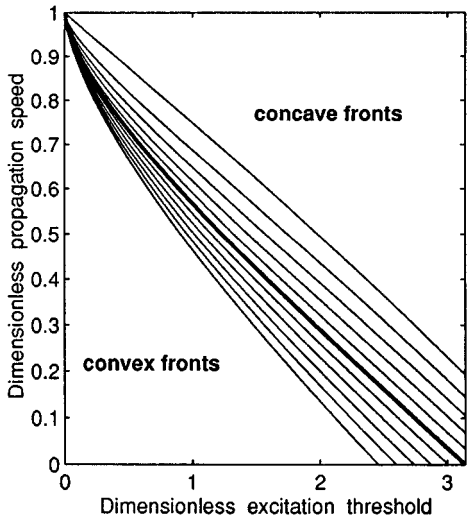

FIG. 11. Dimensionless propagation speed $\hat{c}$ vs dimensionless excitation threshold $\hat{k}$ for selected dimensionless curvatures η according to Eqs. (21). The thick curve corresponds to the plane wave case $\eta=0$ shown in Fig. 9 for two different values of R_d, but now rescaled to a single curve. The value of η ranges from -1 to $+1$ in steps of 0.2 from bottom to top.

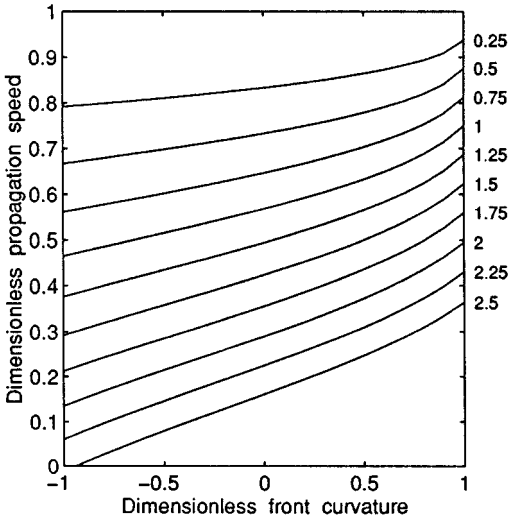

FIG. 12. Propagation speed $\hat{c}$ vs wave-front curvature η for different excitation thresholds $\hat{k}$ (shown on the right) according to Eqs. (21). At each $\hat{k}$, the propagation speed is increased by positive curvature (concave fronts) and decreased by negative curvatures (convex fronts) relative to the plane wave speed $c_0(\hat{k})$ ($\eta=0$).

$$c=\frac{R}{\Delta t}\left\{\cos\frac{\alpha}{2}+\frac{1}{\eta}\left[1-\sqrt{1-\eta^2\sin^2(\alpha/2)}\right]\right\},$$

$$\hat{k}=G_0(\alpha)-\frac{1}{\eta^2}\,G_0(2\arcsin[\,\eta\,\sin(\alpha/2)\,]). \qquad (21)$$

It is readily seen that the second terms in both equations (21) vanish in the limit $\eta\to 0$ (the expression in square brackets is $\sim\eta^2$ and $G_0\sim\eta^3$ when $\eta\ll 1$). The set of equations (21) therefore reduces to expressions (16) and (17) for plane waves as $\eta\to 0$, i.e., as the wave front becomes planar. The family of dimensionless propagation speeds $\hat{c}\equiv c\Delta t/R$ versus the dimensionless excitation thresholds $\hat{k}$ parametrically represented by Eqs. (21) is shown in Fig. 11 for various dimensionless curvatures η. The bold curve in the middle corresponds to the plane wave case $\eta=0$, similar to those shown previously in Fig. 9 for two different values of R_d, but now rescaled to a single curve. Let us show that in the whole domain of validity of the set (18)–(20) the propagation speed always decreases monotonically when the threshold grows at fixed curvature. Taking the derivative of $\hat{c}\equiv c\Delta t/R$ from Eq. (19) we have $2d\hat{c}/d\alpha=-\sin(\alpha/2)(1-d\beta/d\alpha)$. Similarly, using Eq. (20) one can show that $d\hat{k}/d\alpha=2(1-d\beta/d\alpha)\sin^2(\alpha/2)$. Therefore, we obtain at any fixed η,

$$\frac{d\hat{c}}{d\hat{k}}=-\frac{1}{4\sin(\alpha/2)}, \qquad (22)$$

and because $0\leqslant\alpha<2\pi$ we always have $d\hat{c}/d\hat{k}<0$, so $\hat{c}$ is indeed a decreasing function of the threshold $\hat{k}$.

Parametric equations (21) can also be considered at fixed thresholds and represented as a family of propagation speeds versus curvature, each curve marked by a certain value of $\hat{k}$ as displayed in Fig. 12. One can see from the figures that for positive curvatures (concave fronts), the propagation speed at each threshold $\hat{k}$ is increased relative to the plane wave speed, while for negative curvatures (convex fronts) the propagation speed is reduced. The mechanism controlling the speed of curved fronts in the discrete model is analogous to the focusing and defocusing of diffusive flux (a linear process) in continuous media, since the magnitude of the source (the linear sum of excited elements on the front inside R) depends on the curvature. Note that in our calculations with $\eta<0$ we have limited the range of α variation by the requirement that the propagation speed be nonnegative, $c_\cap\geqslant 0$. This imposes the limitation that $\alpha\leqslant\alpha_{\max}(\eta)\equiv 2\arccos(|\eta|/2)$, so α needs to be varied only in the interval $[0,\alpha_{\max}]$.

We performed simulations of curved wave fronts on a two-dimensional lattice. Each lattice element was assigned an identical interaction radius R ($R_d=6$ lattice units) and identical threshold value K. Wave speeds and wave-front curvatures were measured for convex waves by exciting circular domains of elements of varying initial radii R_0 (in lattice units) and computing the average of the radial distance at time t $\langle R_t\rangle$ to points on the wave front (defined by excited elements with at least one adjacent resting neighbor) as the wave propagated outward. The ''instantaneous'' wave speed was given by $(\langle R_{t+\Delta t}\rangle-\langle R_t\rangle)/\Delta t$, while the dimensionless curvature $|\eta|$ was $R_d/\langle R_t\rangle$. A similar procedure was used for concave fronts except we excited the entire lattice and created ''holes'' of resting elements of different sizes R_0. The results for three different K values and the corresponding theoretical curves computed using equations (21) are shown in Fig. 13. The simulation results demonstrate good agreement with the theory. To illustrate the effect of finite T_E, the convex wave simulations for $K=48$ were performed using $T_E=20$ time steps. The result is a minimum nonzero speed below which no convex waves stably propagate [the lowest curve in Fig. 13(a)]. A complete analysis of this effect is the subject of a future study.

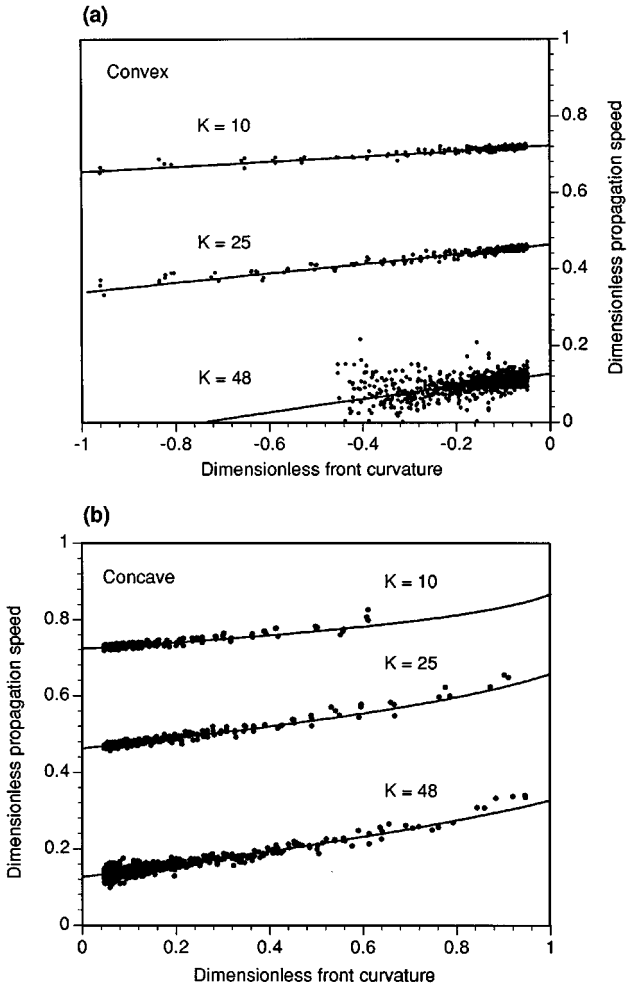

FIG. 13. Measured wave speed $\hat{c}$ vs curvature η for convex (a) and concave (b) fronts. The spatial discretization $R_d=6$. Simulations were performed for three different threshold values $K=10$, 25, and 48, corresponding to the dimensionless thresholds $\hat{k}=0.55$, 1.39, 2.67, respectively. (a) We created small circular domains of excited elements and measured the radius of the excited domain (averaged over seed point locations) as the wave propagated outward; (b) we created large holes of resting elements inside a lattice of fully excited elements and measured the radius of the resting domain (averaged over the seed point locations) as the wave propagated inward. In both (a) and (b), the wave speed was defined as $(|\langle R_{t+\Delta t}\rangle-\langle R_t\rangle|)/\Delta t$ and the dimensionless curvature $|\eta|$ as $R_d/\langle R_t\rangle$ (all radii are measured in lattice units). The large fluctuations for $K=48$ at high convex curvatures are due to the poor statistics at these very slow wave speeds. The theoretical curves were computed using Eqs. (21).

B. Domain of validity

We now wish to analyze the set of equations (18)–(20) for curved wave fronts in the whole domain in which these equations make sense both physically and mathematically. The mathematical considerations require that $c\geqslant 0$, $\hat{k}>0$ and also that the simultaneous choice of angles α and β related by Eq. (18) be consistent with the conditions $|\sin(\alpha/2)|\leqslant 1$ and $|\sin(\beta/2)|\leqslant 1$. All calculations so far are based on the assumption that the wave front can be *locally* approximated by a circle. In the case of convex wave fronts with arbitrary values of $\eta\leqslant 0$, this assumption can be justified even when $|\eta|\gg 1$. For large curvatures $\eta<0$ and $|\eta|\gg 1$, the parameter $-\eta$ can be understood as an inverse of the radius r of the circle, which approximates the wave front globally (as a whole). On the other hand, for concave fronts with curvature $\eta>1$, the overlapping area depends on the entire wave-front shape and cannot be fully described by local curvature. For example, when $\eta>1$ the whole wave front may completely fall inside the interaction region. In this case, the overlapping area completely surrounds the central element and forward propagation of the front is no longer meaningful (the front implodes). In addition to the fact that R is the spatial resolution of the model, this is another important physical reason to disregard $\eta>1$. On the other hand, the local approximation of the wave-front shape as a circle is valid for convex fronts with $|\eta|\gg 1$, so the model's behavior is physically meaningful in this region. In this case, we may need to circumvent the relation of our model to the continuous PDEs and look for a direct link to real physical systems (note that the PDEs are themselves an approximate description of the underlying physical processes in the medium). We thus consider the behavior of our model in the whole curvature range $\eta\in(-\infty,1]$.

C. Critical curvature

In this subsection, we find an expression for the curvature corresponding to vanishing propagation speed (the critical curvature). According to Eqs. (18)–(20), at fixed curvature the propagation speed decreases monotonically when the threshold $\hat{k}$ grows and it eventually vanishes when the threshold reaches a maximum value $\hat{k}_{\max}$. Considering the range of curvature $\eta\in[-2,1]$ and setting $c=0$ in Eq. (21), we readily find that this occurs when $\cos(\alpha/2)=-\eta/2$, or when $\alpha=\alpha_{\max}(\eta)\equiv 2\arccos(-\eta/2)$. It follows that at the critical situation $2\alpha_{\max}-\beta=2\pi(\beta<0)$, which allows us to obtain the maximum threshold value as a function of curvature η in the form

$$\hat{k}_{\max}=H(\eta)\quad(-2\leqslant\eta\leqslant 1),\tag{23}$$

where

$$H(\eta)=2\arccos\left(-\frac{\eta}{2}\right)+\frac{2}{\eta}\left(1-\frac{\eta^2}{4}\right)^{1/2}\mp\frac{2}{\eta^2}\arccos\left(1-\frac{\eta^2}{2}\right),\tag{24}$$

and the minus and plus signs are to be used for $\eta>0$ and $\eta<0$, respectively. As one can see from Eq. (23), the maximum threshold value $\hat{k}_{\max}$ exists and the propagation terminates continuously through ''slowing down'' when $|\eta|\leqslant 2$. Note also that according to Eq. (23) $\hat{k}_{\max}>\pi$ when $\eta>0$ [a concave front can still propagate even when $\alpha_0(\hat{k})$ exceeds π, which is the value corresponding to vanishing plane wave speed]. When $\eta<-2$ the situation becomes more interesting. In this case the propagation terminates at a certain critical nonzero speed as is illustrated in Fig. 14. In all such cases $\beta=2\pi$. Setting $\beta=2\pi$ in (18)–(20), we thus obtain the threshold and the speed at which the propagation of the front with given curvature η terminates:

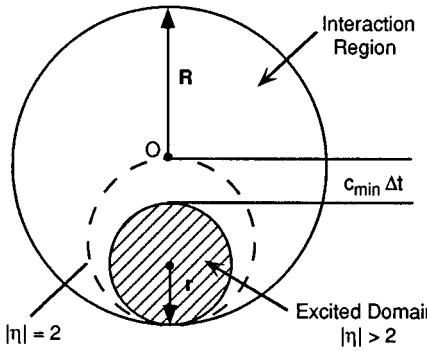

FIG. 14. Geometry for convex wave fronts with $|\eta|=R/r>2$. The critical curvature is associated with a nonzero critical speed $c_{\min}$. When $0\leqslant|\eta|\leqslant 2$ the critical speed $c_{\min}$ is always equal to zero. The case $|\eta|=2$ is shown by the dashed circle.

$$\hat{k}=\hat{k}_{\max}=\frac{2\pi}{\eta^2},\quad \hat{c}=\hat{c}_{\min}=1+\frac{2}{\eta}\quad(\eta\leqslant -2). \tag{25}$$

Figure 15 shows the propagation speed $\hat{c}$ versus threshold $\hat{k}$ for convex fronts with $|\eta|>1$ (the curves 5, 6, and 7 correspond to $|\eta|>2$). The lower parts of the curves correspond to β from the interval $[\pi,2\pi]$ and the end points correspond to $\beta=2\pi$. Comparing Eq. (23) and the first equation in (25), we see that the maximum threshold $\hat{k}_{\max}$ is a continuous function of η, which we plot in Fig. 16(a). The portion of the lower curve to the right of the vertical line $\eta=-2$ is described by Eq. (23) and corresponds to vanishing propagation speed. The portion of the curve to the left of the vertical $\eta=-2$ is described by relations (25) and corresponds to nonzero cutoff speeds. If one sets $\hat{c}_{\min}=0$ for $\eta\geqslant -2$, then the cutoff speed $\hat{c}_{\min}$ becomes a continuous function of η.

It is important to note that the graph in Fig. 16 can also be considered as representing the critical curvature η_{cr} at which propagation terminates for a given threshold $\hat{k}$. As discussed previously, the critical curvature for trigger waves is defined by the requirement $c=0$, so for our CA model the critical curvature must be found from Eq. (23) with $\hat{k}\geqslant\pi/2$.

D. Diffusion constant in the CA medium

In this subsection, we consider the behavior of the CA model in the limit of small curvatures. If we compare each $\hat{c}$ versus η curve in Fig. 12 with that given by expression (8) for continuous media, we see that the slope $d\hat{c}/d\eta$ at $\eta=0$ represents the effective (dimensionless) diffusion constant $\hat{D}$ of the medium, while the $\hat{c}$ intercept corresponds to the speed of a plane wave at threshold $\hat{k}$. As can be observed in Fig. 12, the slopes $\hat{D}$ at small η depend on the specific threshold values $\hat{k}$. We can obtain an explicit expression for this dependence by evaluating (18)–(20) for $\eta\to 0$ within the first order in η. In this approximation, Eq. (18) reduces to $\beta\simeq 2\eta\sin(\alpha/2)$, so the term $[1-\cos(\beta/2)]/\eta\equiv(2/\eta)\sin^2(\beta/4)$ in Eq. (19) becomes $(2/\eta)[\eta/2\sin(\alpha/2)]^2=(\eta/2)\sin^2(\alpha/2)$. Equation (19) thus becomes

$$c=\left(\cos\frac{\alpha}{2}+\frac{\eta}{2}\sin^2\frac{\alpha}{2}\right)\frac{R}{\Delta t}, \tag{26}$$

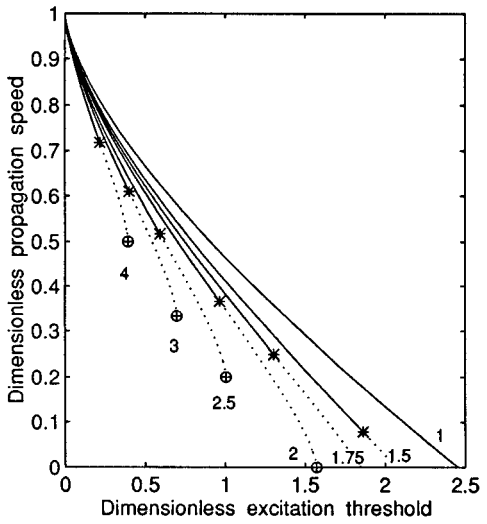

FIG. 15. Propagation speed $\hat{c}$ vs excitation threshold $\hat{k}$ for convex wave fronts with $|\eta|\geqslant 1$ obtained using Eqs. (18)–(20). The values of η are marked next to the curves. The dashed portions of the curves are computed for β in the interval $[\pi,2\pi]$. These end points are highlighted in the figure by an asterisk and the $\oplus$ symbol, respectively. Note that for convex fronts with $|\eta|\geqslant 2$, wave propagation terminates at a critical nonzero speed (see geometry in Fig. 14).

and because $G_0(\beta)\simeq\beta^3/6$ for small $\beta\sim\eta$, expression (20) reduces to

$$\hat{k}=\alpha-\sin\alpha-\frac{4}{3}\,\eta\,\sin^3\frac{\alpha}{2}. \tag{27}$$

When the curvature is small we have $\alpha=\alpha_0+\Delta\alpha$, where the angle α_0 corresponds to the plane wave case and $\Delta\alpha$ is of the order of η. Therefore within the same precision one can replace α by α_0 in the second term in Eq. (26) and in the last term in Eq. (27). To obtain from Eq. (26) an expression similar to Eq. (8), we just need to find the first two terms of expansion of c in the power series in η. Substituting $\alpha=\alpha_0+\Delta\alpha$ into Eq. (27) and using Eq. (17) we have $(1-\cos\alpha_0)\Delta\alpha-\frac{4}{3}\eta\sin^3(\alpha_0/2)\simeq 0$, which yields $\Delta\alpha=\frac{2}{3}\eta\sin(\alpha_0/2)$. Using this expression and the fact that $\cos(\alpha/2)\simeq\cos(\alpha_0/2)-(\Delta\alpha/2)\sin(\alpha_0/2)$ we may reduce Eq. (26) to

$$c=\left(\cos\frac{\alpha_0}{2}-\frac{\eta}{6}\sin^2\frac{\alpha_0}{2}\right)\frac{R}{\Delta t}. \tag{28}$$

Recalling Eq. (16) and the fact that $\eta=R\kappa$, where κ is the usual dimensional curvature, we finally obtain the following expression for the speed of the curved front in the region of small curvatures:

$$c=c_0+\left\{\frac{R^2}{6\Delta t}\sin^2\frac{\alpha_0}{2}\right\}\kappa, \tag{29}$$

where α_0 is the angular threshold, which can be expressed in terms the usual threshold K or $\hat{k}$ defined in Eq. (17). Comparison of Eq. (29) with Eq. (8) requires that the expression in the curly brackets be identified with the diffusion coefficient D of the continuous PDE model:

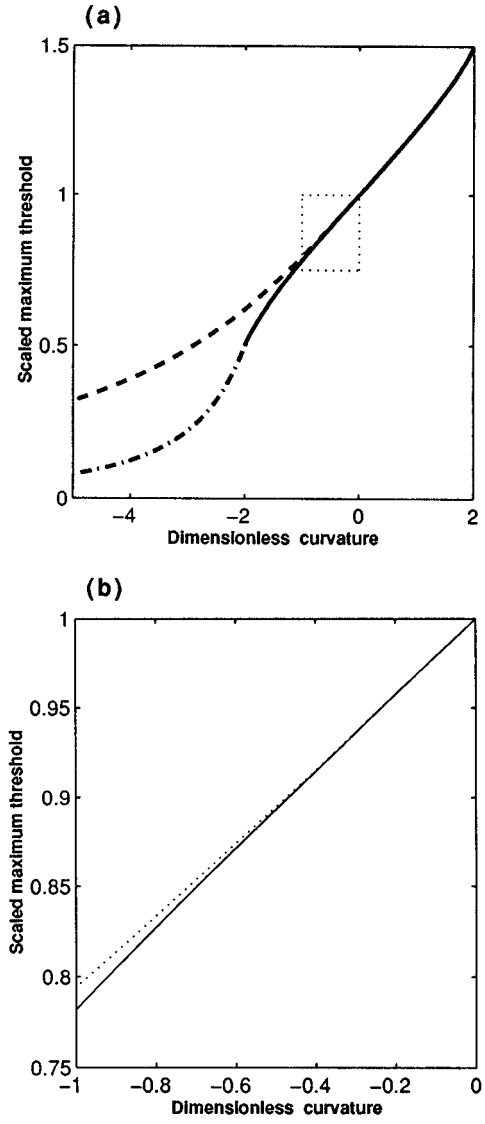

FIG. 16. Maximum excitation threshold $\hat{k}_{\max}/\pi$ vs curvature η. (a) The solid portion of the curve is obtained using Eq. (23) and corresponds to the case $c_{\min}=0$, while the dashed portion ($\eta<-2$) corresponds to nonzero cutoff speeds given by Eq. (25). This curve may also be interpreted as the critical curvature $\eta_{\rm cr}$ as a function of excitation threshold $\hat{k}$. The dashed line represents the estimated $\hat{k}_{\max}$ obtained using a linear speed vs curvature relation with slope $\hat{D}=d\hat{c}/d\eta|_{\eta=0}$ and intercept $\hat{c}_0$. (b) Close up of the region indicated by the square in (a).

$$D=\frac{R^2}{6\Delta t}\sin^2\frac{\alpha_0(\hat{k})}{2},\quad \alpha_0(\hat{k})\equiv G_0^{-1}(\hat{k}),\qquad (30)$$

where G_0^{-1} is the inverse of the function G_0 defined by Eq. (17). In accordance with our derivation, this expression for D is valid for small values of η ($\kappa\ll 1/R$), and can be expected to hold up to moderate $\eta\sim 1$. For fixed R and Δt, the effective diffusion constant D is a monotonically increasing function of threshold $\hat{k}$ and is shown in dimensionless form ($\hat{D}=D\Delta t/R^2$) in Fig. 17. The points ($\odot$ symbols) on the graph were obtained by numerically evaluating the slopes of the curves shown in Fig. 12 at $\eta=0$. The slopes in the linear region agree well with the theoretical values of $\hat{D}$. The fact

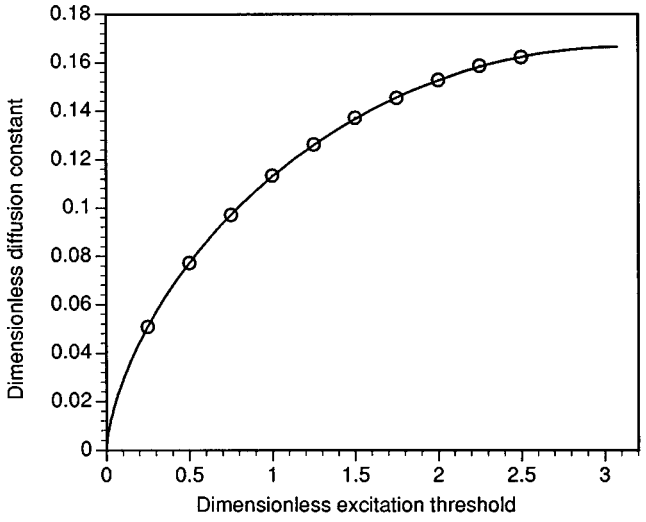

FIG. 17. The dimensionless diffusion constant $\hat{D}\equiv D\Delta t/R^2$ of the CA model as a function of excitation threshold $\hat{k}$ according to Eq. (30). The points indicated by the $\odot$ symbol were obtained by numerically evaluating the slopes of the curves shown in Fig. 12 at $\eta=0$.

that both D and c_0 depend on the parameter $\hat{k}$ [as seen from Eqs. (16), (17), and (30)] implies that *these values may not be varied independently* when R and Δt are held fixed. If we wish to vary the local propagation speed at fixed time step Δt, we must restrict the variations of R and K to the surface $D(R,K)=$const, that is, we must vary R and K in such a way that D remains fixed. This is because D is a constant of the medium.

In the previous three sections, we established the framework for relating the trigger wave solutions of the PDE and CA representations of the medium. We are now in a position to formulate the requirements for representing a continuous medium using a CA model. In the remainder of the paper, we discuss this methodology and use it to write and solve the equations for the CA parameters values corresponding to given PDEs. We realize this program for two specific PDE models of an excitable medium.

V. CORRESPONDENCE

This section discusses the specific procedure for finding the CA parameter values for an excitable medium described by a specific set of PDEs. These values are found via solution of the set of equations obtained by equating the CA model expressions for the plane wave speed c_0, critical curvature $\kappa_{\rm cr}$, and diffusion constant D to the corresponding PDE values. For a given spatial discretization R_d, this yields a set of three equations for the three unknown CA model quantities: R, K, and Δt. Each solution of these equations must be unique, therefore the CA parameter values may not be varied independently.

The correspondence between the trigger wave solutions of the CA model and those of the PDEs can be seen more directly by comparing the respective space scales L_0 and time scales τ_0 for propagating plane waves with one another. Using expression (16) for the plane wave speed and Eq. (30) for the effective diffusion constant, we obtain the expres-

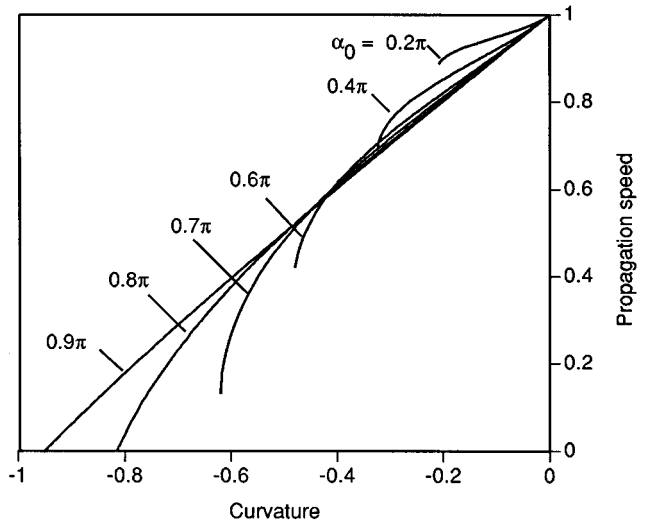

FIG. 18. Propagation speed (in units of L_0/τ_0) vs curvature (in units of $1/L_0$) for different values of the angular threshold α_0 according to Eqs. (31) and (32). In these units the plane wave speed C_0 and diffusion constant D are equal to 1.0 for all α_0. We see that the shape of the curves and the critical curvature depend sensitively on α_0. For sufficiently large α_0, the relation is approximately linear up to moderate wavefront curvatures.

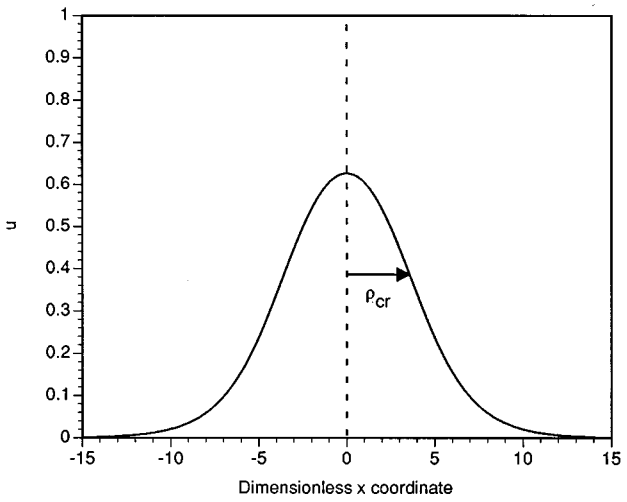

FIG. 19. A cross section through the two-dimensional critical (stationary) wave profile $u_{cr}(\rho)$ obtained for the FN model ($\varepsilon=0$) with $a=0.25$ and $D=1.0$. The critical radius of curvature ρ_{cr} is 3.66 and is indicated by the arrow. The corresponding critical curvature $\kappa_{cr}\equiv -1/\rho_{cr}$ is -0.273.

sions for $L_0=D/C_0$ and $\tau_0=D/C_0^2$ in the CA medium:

$$\tau_0=\Delta t\,\frac{\tan^2[\alpha_0(\hat{k})/2]}{6}, \tag{31}$$

$$L_0=R\,\frac{\sin^2[\alpha_0(\hat{k})/2]}{6\cos[\alpha_0(\hat{k})/2]}, \tag{32}$$

where the angular threshold $\alpha_0(\hat{k})$ is the inverse of the function $G_0(\alpha_0)$ defined in Eq. (17). We see that the interaction radius R is proportional to the wave-front space scale L_0 and the time step Δt is proportional the wave-front formation time τ_0, where the proportionality constants depend on the specific excitability [the dimensionless angular threshold $\alpha_0(\hat{k})$] of the medium. For given PDE values of the plane wave speed C_0 and diffusion coefficient D, Eqs. (31) and (32) determine R and Δt for each value of the angular threshold α_0 (or threshold $\hat{k}$). Note that for varying α_0, each solution of these equations automatically satisfies the constraint $D(R,K)=$const, where const is the PDE model diffusion coefficient D. Since $R=R_d\Delta x$, either R_d or Δx may be chosen freely, but their product must satisfy Eq. (32). Generally, we want to choose R_d as large as computational resources will allow. The third relation, which fixes the value of α_0, is found by matching the critical curvatures in the PDE and CA representations.

To see the relationship between the angular threshold $\alpha_0(\hat{k})$ and the critical curvature more clearly, we first define two new dimensionless quantities $R'\equiv R/L_0$ and $\Delta t'\equiv\Delta t/\tau_0$. If we substitute these rescaled quantities into Eqs. (16) and (30), we see that in these units $C_0'=1$ and $D'=1$, independent of the value of α_0. In Fig. 18, we plot the wave speed versus wave-front curvature for convex fronts in these units for selected values of α_0. When α_0 is large (low excitability), the relation is approximately linear over a broad range of curvatures, but the shape of the curve in the nonlinear region and the value of the critical curvature depend strongly on α_0. For trigger waves, the solution value of α_0 must lie in the range $0.74\pi\leqslant\alpha_0\leqslant\pi$ (corresponding to $\pi/2\leqslant\hat{k}\leqslant\pi$), since the trigger wave speed at $\kappa=\kappa_{cr}$ must vanish (this is equivalent to the condition that the dimensionless critical curvature η_{cr} satisfy $\eta\geqslant -2$).

To find α_0, recall that Eq. (23) can be interpreted as the dependence of the critical curvature η_{cr} on the dimensionless threshold $\hat{k}$ and can be written as $\hat{k}=H(\eta_{cr})$, where the function H is defined by Eq. (24). Expressing $\hat{k}$ in this relation as $G_0(\alpha_0)$ and setting $\eta_{cr}=R\kappa_{cr}$ we obtain

$$G_0(\alpha_0)=H(R\kappa_{cr}), \tag{33}$$

where the constant κ_{cr} is the specific PDE solution value. This equation must be solved simultaneously with Eqs. (31) and (32), which uniquely determines all three parameters R, K, and Δt. Since we only match the PDE and CA model wave speed versus curvature plot at two points (A and B in Fig. 2) and a slope (at $\kappa=0$), we expect that the correspondence will not be exact in the nonlinear regions of these curves, but we do expect the CA model relation to interpolate the PDE values in this region reasonably well.

A. Examples

The FitzHugh-Nagumo model (FN) [14,15] is a simple model of an excitable medium often used to study traveling wave patterns in neuromuscular tissue. In a two-dimensional homogeneous and isotropic medium, the FN model in the appropriate limit may be obtained from Eqs. (3) and (4) with $f(u,v)$ given by a cubic polynomial and $\varepsilon=0$ (the latter allows us to set v to the initial, resting value $v_s=0$). In dimensional form and using a specific normalization [53] this yields

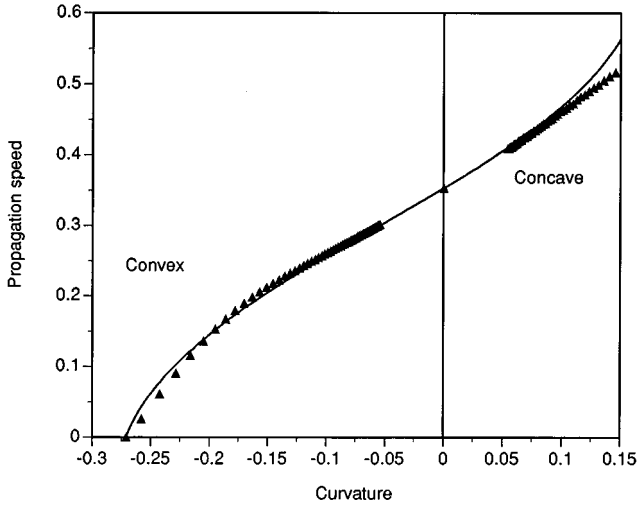

FIG. 20. Measured propagation speed C (triangles) vs curvature κ in the FitzHugh-Nagumo (FN) medium with $D=1.0$ and $a=0.25$. The curve is the computed theoretical CA model relation for these specific PDE parameter values. The average value of the FN wave speed was computed by tracking the position of the inflection point of the wave front at each time step. For convex fronts, the points were obtained by perturbing the critical profile $u_{\rm cr}$ and following its evolution. The points are identical to those shown in Fig. 2. For concave wave fronts, the initial configuration consisted of a lattice of excited nodes ($u=1.0$) with a large central hole of resting nodes ($u=0.0$). This configuration was first allowed to evolve until the wave front fully formed. The end point of the CA model curve at positive κ is found by setting $\beta=\pi$ in (18), (19), and (20). This is the maximum value of β for which forward propagation of a concave wave front is meaningful. The space step and time steps for the PDEs were chosen to be $h=0.25$ and $\delta t=0.001$. The measured plane wave speed in PDEs using these values was $C_0=0.353$ in good agreement with the theoretical value 0.354. The agreement is excellent over a broad range of curvatures.

$$\frac{\partial u}{\partial t}=D\nabla^2 u+u(a-u)(u-1), \tag{34}$$

where a is a positive constant ($0<a<1/2$). The nonlinear eigenvalue problem (5),(6) for trigger waves in the FN model (34) has a simple analytic solution with the plane wave speed given by $C_0=(D/2)^{1/2}(1-2a)$ [53]. The plane wave speed C_0 is a decreasing function of a, which plays the role of the excitation threshold. Below, we use the specific parameter values $a=0.25$ and $D=1.0$, which gives a theoretical value of the plane wave speed $C_0=0.35$.

To find the critical curvature $\kappa_{\rm cr}$ for these parameter values, we recall from Sec. II that the critical radius $\rho_{\rm cr}$ can be defined as the ρ value of the maximum of the probability density $p(\rho)$ defined in Eq. (10), i.e., $p(\rho_{\rm cr})=\max$. In the case under consideration, $\rho_{\rm cr}$ also represents the position of the inflection point of the stationary wave profile at which $u''(\rho_{\rm cr})=0$. To find $\rho_{\rm cr}$, we solved Eq. (9) numerically for $u_{\rm cr}(\rho)$ by matching numerical solutions to the asymptotic analytical solutions near $\rho=0$ and $\rho=\infty$. At infinity the source can be linearized and we have $u_{\rm cr}(\rho)\sim K_0(\sqrt{s_1}\rho)$, where K_0 is the cylindrical function of imaginary argument (McDonald function) and $s_1=-df(0)/du$. This procedure yielded $u_{\rm cr}(\rho=0)\approx 0.6269$ with the inflection point located at

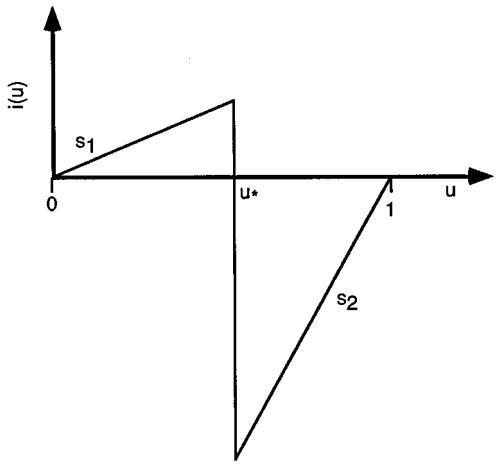

FIG. 21. The piecewise linear current $i(u)$ commonly used in simplified (caricature) PDE models of neuromuscular tissue [the reaction source $f(u)=-i(u)$]. The slopes of $i(u)$ for $u<u_*$ and $u>u_*$ are s_1 and s_2, respectively. The quantity u_* plays the role of the local excitation threshold.

$\rho_{\rm cr}=3.66$, thus $\kappa_{\rm cr}\equiv -1/\rho_{\rm cr}=-0.27$. A cross section through the critical profile is shown in Fig. 19.

We calculated the corresponding CA model parameter values using the method described above and obtained $R=6.62$, $\Delta t=6.43$, and $\hat{k}=1.79$. For a spatial discretization $R_d=12$ this gives $K=129$ elements. We see that the value of R is of the order of the wave-front space scale $L_0=2.83$ (actually L_0 underestimates the wave front width since it more closely approximates the smaller length constant of the foot of the wave), and Δt is of the order of the front formation time $\tau_0=8.0$. To check the correspondence between the PDE and CA model representations, we solved the FN equation (34) numerically for the evolution of a perturbed critical wave-front profile $u_{\rm cr}(\rho)$ on a two-dimensional square lattice with no flux boundary conditions. The numerical solutions were obtained using explicit Euler integration for the reaction term $f(u)$ and an explicit forward time centered finite difference scheme for the diffusion term [54]. The nine-point Laplacian formula [55] used gives a rotationally invariant Laplacian to $O(h^4)$, where h is the lattice spacing [56]. We used the values $h=0.25$ for the grid spacing and $\delta t=0.001$ for the time step. The wave speed was estimated by tracking the motion of the inflection point on the lattice. The theoretical CA model speed-curvature relation and the numerical solution of the PDEs is shown in Fig. 20. The CA model relation interpolates the PDE solution values quite well.

As another illustration, we now consider the case of the commonly used piecewise linear current source $i(u)$ [40,22,41] shown in Fig. 21. For this case, the reaction term $f(u)$ is given by

$$f(u)=-i(u)=-\begin{cases} s_1 u & \text{when } u<u_* \\ s_2(u-1) & \text{when } u\geqslant u_*, \end{cases} \tag{35}$$

where without loss of generality v has been set to zero. The constants s_1, s_2 are the slopes, and u_* plays the role of the excitation threshold ($0<u_*<1$). The solution of the nonlinear eigenvalue problem (5),(6) for the dimensionless plane wave speed $\hat{c}_0$ is [40–42]

$$\hat{c}_0=\sqrt{s_2}\,\frac{(1-u_*)^2-u_*^2\lambda}{\sqrt{u_*(1-u_*)[1-u_*(1-\lambda)]}}\quad(\lambda\equiv s_1/s_2). \tag{36}$$

The solution for the critical profile $u_{\rm cr}(\rho)$ is obtained by solving Eq. (9) with the source (35) under the condition that $u_{\rm cr}$ is bounded in the domain $0<\rho<\infty$. We shall use the new variable $\hat{u}\equiv 1-u(\rho)$ in the region $u\geqslant u_*$ and utilize the variable u in the region of the foot (leading edge) of the wave where $u<u_*$. The function $u_{\rm cr}(\rho)$ is thus determined by the equations

$$\frac{d^2u}{d\rho^2}+\frac{\nu}{\rho}\frac{du}{dr}-s_1u=0\quad\text{when}\quad u<u_*, \tag{37}$$

$$\frac{d^2\hat{u}}{d\rho^2}+\frac{\nu}{\rho}\frac{d\hat{u}}{dr}-s_2\hat{u}=0\quad\text{when}\quad u\geqslant u_*. \tag{38}$$

The equations in both the exterior (37) and interior (38) regions are linear differential equations with singular points at $\rho=0$ and $\rho=\infty$. A solution of such an equation is a linear combination of two solutions out of which one is singular near $\rho=0$ and bounded near $\rho=\infty$, and vice versa. The requirement that the solutions are bounded implies that in the inner solution ($u\geqslant u_*$, the region including $\rho=0$) only the term regular at $\rho=0$ is retained, whereas in the outer solution ($u<u_*$, the region including $\rho=\infty$) only the term bounded at $\rho=\infty$ is retained. This leaves us with two integration constants, one for each region. A solution of a differential equation of the second order must be continuous together with its derivative on the entire interval, including the point where $u=u_*$. This smoothness condition generates two equations for the two integration constants, which allows us to eventually find $u_{\rm cr}(\rho)$.

Similar to the above FN case, we define the critical radius $\rho_{\rm cr}$ by the condition $p(\rho_{\rm cr})=\max$. Note that the discontinuous source (35) gives rise to a wave profile that does not possess an inflection point, and therefore $\rho_{\rm cr}$ cannot represent this point anymore. However, it is not difficult to show that the maximum of the distribution $p(\rho)$ is reached exactly at the matching point of the inner and outer solutions, where $u_{\rm cr}$ reaches the value u_*. Thus, the critical radius $\rho_{\rm cr}$ is determined by the equation

$$u_{\rm cr}(\rho_{\rm cr})=u_*. \tag{39}$$

After some transformations, the matching conditions together with relation (39) reduce to a simple transcendental equation for $\rho_{\rm cr}$ that takes different forms in the case of two ($\nu=1$) and three ($\nu=2$) dimensions. In both cases the equation is formulated in terms of the renormalized critical radius $r_*\equiv\rho_{\rm cr}\sqrt{s_2}$ and in the two-dimensional case has the form

$$\frac{I_1(r_*)}{I_0(r_*)}=\frac{\sqrt{\lambda}u_*}{1-u_*}\,\frac{K_1(\sqrt{\lambda}r_*)}{K_0(\sqrt{\lambda}r_*)}, \tag{40}$$

where $\lambda=s_1/s_2$, and I_n and K_n are the cylindrical functions of imaginary argument and n ($n=0,1$) is the order of the cylindrical function (I_n are modified Bessel functions and K_n are McDonald functions). In the three-dimensional case, the equation for the critical radius assumes the elementary form

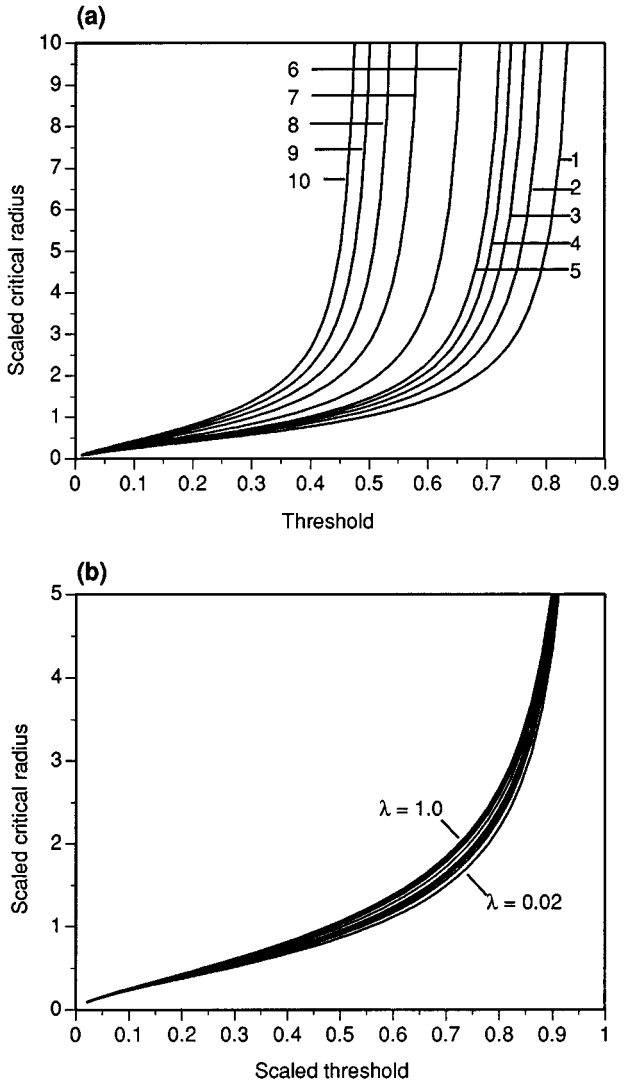

FIG. 22. (a) The renormalized critical radius $r_*=\sqrt{s_2}\rho_{\rm cr}$ vs threshold u_* for selected values of the slope ratio $\lambda=s_1/s_2$ of the piecewise linear current $i(u)$. The λ values of the curves labeled 1–10 are 0.02, 0.04, 0.06, 0.08, 0.1, 0.2, 0.4, 0.6, 0.8, and 1.0, respectively. (b) Renormalized critical radius vs the rescaled threshold parameter $u_*(1+\sqrt{\lambda})$. The curves in (b) illustrate that r_* depends approximately on a *single* lumped parameter of $i(u)$.

$$\tan r_*=\frac{(1-u_*)r_*}{1+u_*r_*\sqrt{\lambda}}. \tag{41}$$

It can be readily shown that each of the equations (40) and (41) has a unique positive solution r_* (under some unrestrictive conditions). Thus, the smoothness conditions allow us to explicitly find $u_{\rm cr}(\rho)$ and determine the values of $\rho_{\rm cr}=r_*/\sqrt{s_2}$ and $\kappa_{\rm cr}\equiv-1/\rho_{\rm cr}$. Numerical solutions of equations (40) are plotted in Fig. 22(a) as $r_*=\sqrt{s_2}\rho_{\rm cr}$ versus u_* for several values of λ. Figure 22(b) shows r_* plotted versus the rescaled threshold value $u_*(1+\sqrt{\lambda})$. The overlap of these curves illustrates that r_* depends approximately on a single ''lumped'' parameter of the nonlinear source $i(u)$.

To compare the solutions of the PDEs with piecewise linear source to the CA model simulations, we chose the specific case $s_1=0.25$, $s_2=0.75$ (which are identical to the

end slopes in FN case considered above) and $u_* = 0.25 = a$ (which is the same threshold value as the FN case). In the chosen units $D = 1.0$. We tracked the evolution of two circular regions of excited elements with initial radii slightly larger than the critical curvature radius $-1/\kappa_{cr}$ in both models. To ensure that the initial configurations were identical, the circular regions (with u set equal to 1) in the PDE system were first evolved until the wave fronts fully formed, then the position of the wave front (the locus of points with $u = u_*$) was used to set the initial configuration of excited elements in the CA model. The numerical PDE solution and the CA simulations are shown in Fig. 23. In the first two snapshots (a) and (b), the waves emanating from each circular region evolve through large negative curvatures as they expand outward. These wave fronts eventually collide with one another, creating a single wave front with two cusps [snapshot (c)]. These cusp regions have large positive curvatures, which quickly dissipate as the combined wave front propagates outward [snapshot (d)]. The agreement between the numerical solution of the PDEs and the CA simulations is quite good.

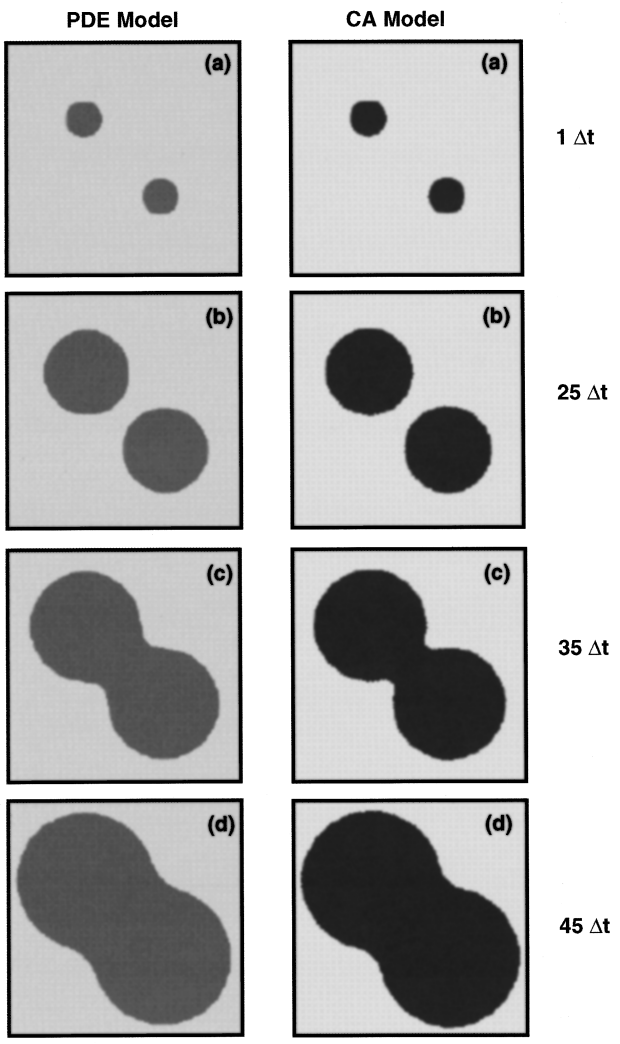

FIG. 23. Evolution of two excited circular domains in the CA model and a PDE model with piecewise linear source and $\varepsilon = 0$. The PDE model parameters were $s_1 = 0.25$, $s_2 = 0.75$, $u_* = 0.25$, and $D = 1.0$, which according to Eq. (36) gives a plane wave speed $C_0 = 1.186$. The value of the critical curvature κ_{cr} was obtained from solution of Eq. (40), which yielded $\kappa_{cr} = -1.12$. We solved for the required CA model parameter values using Eqs. (31), (32), and (33) and obtained $R = 0.86$, $\Delta t = 0.12$, and $\alpha_0 = 0.89\pi$. We chose $R_d = 12$ for the spatial discretization. The space step h and time step δt for the numerical PDE solutions were chosen to be $h = R/R_d = 0.072$ and $\delta t = 0.01 \cdot \Delta t = 0.0012$. In the PDE solutions (left), the light gray and dark gray regions correspond to $u < u_*$, and $u \geq u_*$, respectively. In the CA model simulations (right), resting elements are shown in light gray and excited elements in dark gray. In (a) and (b), the circular waves evolve through large negative curvatures as they propagate outward. The collision at $t \approx 30\Delta t$ produced a single wave front with two cusps as shown in (c). Each cusp has a large positive curvature, which dissipates rapidly as the combined wave front propagates outward (d). The CA model simulations and the numerical solutions of the PDEs agree very well.

B. Inhomogeneities

The most striking feature of the matching procedure used in the previous subsection is that it yields unique values for all CA model parameters, including the time step Δt. In a homogeneous medium, such a restriction presents no difficulty since the model time step Δt will be identical at all locations in lattice. On the other hand, in a medium with spatially varying excitability, the time step Δt becomes *a local quantity*. Since Δt must have a fixed value for all model elements, Eqs. (31) and (32) can only be satisfied for given local values of τ_0 and L_0 if the angular threshold α_0 is determined by these equations alone. This means that its value can no longer be adjusted to obtain the correct local critical curvature. However, as can be seen in Fig. 18, when α_0 is sufficiently large (the cases we are interested in), the speed-curvature relation is approximately linear over a broad range of curvatures, and thus for small and moderate curvatures the value of the propagation speed as a function of curvature is controlled by just two parameters: the slope D and intercept C_0. Therefore, the discrepancy introduced by varying α_0 can be expected to be negligible if the wave configurations do not incorporate regions with large curvature. These same considerations also apply to media with a spatially varying diffusion constant D. We conclude that our minimum CA model can also simulate trigger waves in spatially inhomogeneous media, provided the local wave-front curvatures are not too close to the local critical curvature κ_{cr}.

C. Other discrete models

Gerhardt, Schuster and Tyson (GST) [32,12] recently obtained a set of relations between a CA model and a PDE model of an excitable medium. Their analysis yielded approximate expressions for the CA model's plane wave speed c_0 and effective diffusion constant D in terms of the model's internal parameters. These relations permitted them to obtain a ''reasonably good'' simulator of the Belousov-Zhabotinskii (BZ) reaction that compared favorably with the ''Oregonator'' [57] PDE model of the reaction and experiments. Their result was an important conceptual breakthrough. On the other hand, the validity of the expressions they obtained was undermined by the underlying (artifactual) anisotropy in their model (as discussed by the authors), and also by the fact that their expression for D was found by regression of simulation data: they measured the slopes

$(dc/d\kappa)|_{\kappa=0}$ and averaged over the values obtained for different thresholds K at fixed neighborhood size [32,12] (the threshold dependence of D was thus averaged out). We found that D is a strong function of the threshold K (Fig. 17). Weimar *et al.* [51] later showed that a similar dependence holds in the GST model. In the GST model simulations in Ref. [12], the threshold K was a dynamically varying quantity, thus the model's internal D value could not have remained constant. This is because according to Eq. (30), the neighborhood size R and threshold K must be varied simultaneously to keep D constant when the time step Δt is held fixed. This deficiency in the GST approach was addressed in the more recent work of Weimar, Tyson, and Watson [58], where a specific ''mask'' (similar to our weighting distribution w_{jk}) was chosen that flattens the K dependence of D. We should also point out that the matching procedures used by GST and Weimar *et al.* do not consider the critical curvature, which plays an important role in vortex dynamics, or the fact that the slope of the speed-curvature relation is only identical to the diffusion coefficient of the propagating species in the $\varepsilon=0$ limit (for nondiffusing v variable). In models that incorporate recovery (ε nonzero), the value of the slope depends on ε (though this correction may actually be small).

Using a fundamentally different CA modeling approach, Ito [13] obtained expressions for C_0, D, and also the critical curvature $\kappa_{\rm cr}$. In Ito's model, the wave speed is controlled by varying the propagation speed of a source ''signal'' between the CA elements, rather than by varying the local excitation threshold as required by the parabolic (diffusion-type) PDEs of excitable media. In such a model, a variation in the local excitability is tantamount to a local rescaling of time. This approach can result in unphysical or artifactual behavior that is inconsistent with the PDE description of the medium (though this was admittedly not Ito's stated purpose). For example, the wave speed versus wave-front curvature relation arising in the model is multiple valued in a certain range of excitabilities, which does not appear to be consistent with PDE solutions for typical excitable media (see also our comments below). Also, the critical curvatures $\kappa_{\rm cr}$ are calculated for vanishing propagation speed $c=0$ (the case considered in this paper for trigger waves). As discussed previously, such solutions only exist in the $\varepsilon=0$ limit. Since Ito's model explicitly incorporates the effects of a recovery process (ε nonzero), the computed critical curvatures cannot be compared to values in real physical media.

D. PDEs and discrete modeling philosophy

Finally, we note that in order to develop a physically self-consistent discrete model linked to solutions of PDEs, we must choose a sensible modeling philosophy. The theory of partial differential equations classifies all continuous field processes into three categories as described by elliptic, parabolic, and hyperbolic PDEs. Elliptic PDEs, similar to Laplace's equation describe equilibrium states of continuous systems. Parabolic equations, similar to diffusion or thermoconductivity equations, describe relaxation to equilibrium. Hyperbolic PDEs, similar to the d'Alembert wave equation, describe propagating (causal) processes, which possess intrinsic local propagation velocity. Reaction-diffusion equations describing excitable media are typical parabolic PDEs that do not incorporate any intrinsic propagation speed. The propagation speed observed is determined by the subtle interplay between local sources and sinks and is also affected by the boundary conditions. The underlying process in Ito's model, sending a signal with a given speed, is a process described by a hyperbolic wave equation and can hardly correctly correspond to a physically distinct parabolic process. In contrast, the plane wave speed in our CA model is determined by the condition that the source strength Q equal the magnitude of the sink (the threshold K). Indeed, according to Eq. (30), the model's interaction length R and interaction time Δt for a propagating wave have proven to be linked by a constant D with the dimensions of a diffusion coefficient.

ACKNOWLEDGMENTS

The authors would like to thank Paul Belk, Linda Rosenband, and Joseph Starobin for many useful discussions. This research was supported by NASA Grant No. NAGW-3927 and a grant from the Nihon Kohden Corporation. A.B.F. is also grateful for funding provided by Professor Richard Wilson through a medical physics grant to Harvard University.

[1] A. L. Hodgkin and A. F. Huxley, J. Physiol. **117**, 500 (1952).
[2] C. Luo and Y. Rudy, Circ. Res. **74**, 1071 (1994).
[3] B. P. Belousov, in *Sbornik Referatov po Radiatsionni Meditsine* (Medgiz, Moscow, 1958).
[4] M. Zhabotinskii, Biophys. **9**, 329 (1964).
[5] R. J. Field and R. M. Noyes, J. Am. Chem. Soc. **96**, 2000 (1974).
[6] A. T. Winfree, Science **175**, 634 (1972).
[7] Y. V. Gulyaev, Y. D. Kalafati, L. A. Ryabova, and I. A. Serbinov, Dokl. Acad. Nauk **256**, 357 (1981) [Sov. Phys. Dokl. **26**, 52 (1981)].
[8] D. Mollison, J. R. Stat. Soc. **39**, 283 (1977).
[9] A. J. Durston, J. Theor. Biol. **42**, 483 (1973).
[10] J. R. Weimar and J. Boon, Phys. Rev. E **49**, 1749 (1994).
[11] M. Markus and B. Hess, Nature **347**, 56 (1990).
[12] M. Gerhardt, H. Schuster, and J. J. Tyson, Physica D **46**, 416 (1990).
[13] H. Ito, Physica D **79**, 16 (1994).
[14] R. FitzHugh, Biophys. J. **1**, 445 (1961).
[15] J. S. Nagumo, S. Arimoto, and S. Yoshizawa, Proc. IEEE **50**, 2061 (1962).
[16] P. Fife, SIAM-AMS Proc. **10**, 23 (1976).
[17] J. J. Tyson and J. P. Keener, Physica D **32**, 327 (1988).
[18] E. Meron, Phys. Rep. **218**, 1 (1992).
[19] J. P. Keener, J. Math. Biol. **29**, 629 (1991).
[20] P. Colli-Franzone, L. Guerri, and S. Rovida, J. Math. Biol. **28**, 121 (1990).
[21] V. A. Davydov, V. S. Zykov, and A. S. Mikhailov, Usp. Fiz. Nauk. **61**, 45 (1991) [Sov. Phys. Usp. **34**, 665 (1991)].
[22] A. S. Mikhailov and V. Z. Zykov, Physica D **52**, 379 (1991).
[23] J. Starobin and C. F. Starmer, Phys. Rev. E **54**, 430 (1996).

[24] M. Courtemanche and A. T. Winfree, Int. J. Bif. Chaos **1**, 431 (1991).
[25] A. V. Panfilov and A. V. Holden, Phys. Lett. A **151**, 23 (1990).
[26] J. J. Tyson and P. C. Fife, J. Chem. Phys. **73**, 2224 (1980).
[27] J. P. Boon, D. Dab, R. Kapral, and A. Lawniczak, Phys. Rep. **273**, 1 (1996).
[28] N. Wiener and A. Rosenblueth, Arch. Inst. Cardiol. Mex. **16**, 205 (1946).
[29] J. M. Greenberg and S. P. Hastings, SIAM J. Appl. Math. **34**, 515 (1978).
[30] G. K. Moe, W. C. Rheinboldt, and J. A. Abildskov, Am. Heart. J. **67**, 200 (1964).
[31] J. M. Smith and R. J. Cohen, Proc. Natl. Acad. Sci. **81**, 233 (1984).
[32] M. Gerhardt, H. Schuster, and J. J. Tyson, Physica D **46**, 392 (1990).
[33] J. P. Keener, SIAM J. Appl. Math. **39**, 528 (1980).
[34] J. C. Neu and W. Krassowska, Crit. Rev. Biomed. Eng. **21**, 137 (1993).
[35] Yu. M. Kokos and V. I. Krinsky, Biofizika **18**, 506 (1973).
[36] V. I. Krinsky and Yu. M. Kokos, Biofizika **18**, 878 (1973).
[37] V. I. Krinsky and Yu. M. Kokos, Biofizika **18**, 1067 (1973).
[38] J. P. Keener, SIAM J. Appl. Math. **46**, 1039 (1986).
[39] A. B. Feldman, Y. B. Chernyak, and R. J. Cohen, IEEE Proc. Ann. Int. Conf. IEEE/EMBS **17**, 21 (1995).
[40] A. S. Mikhailov, *Foundations of Synergetics* (Springer-Verlag, New York, 1990).
[41] J. Starobin, Y. I. Zilberter, and C. F. Starmer, Physica D **70**, 321 (1993).
[42] Y. B. Chernyak (unpublished).
[43] Y. B. Chernyak, IEEE Proc. of Ann. Int'l. Conf. of IEEE/EMBS **18** (1996).
[44] R. D. Benguria and M. C. Depassier, Phys. Rev. Lett. **77**, 1171 (1996).
[45] Ya. B. Zeldovich, *Lectures on Combustion Theory* (Gostekhteorizdat, Moscow, 1944); Ya. B. Zeldovich *et al.*, *The Mathematical Theory of Combustion and Explosions* (Consultants Bureau, New York, 1985).
[46] V. S. Zykov and A. A. Petrov, Biofizika **22**, 300 (1978).
[47] R. Kapral, J. Math. Chem. **6**, 113 (1991).
[48] *Theory and Applications of Cellular Automata*, edited by S. Wolfram (World Scientific, Singapore, 1986).
[49] B. E. H. Saxberg and R. J. Cohen, in *Theory of Heart* (Springer-Verlag, New York, 1991).
[50] M. Markus, M. Krafczyk, and B. Hess, in *Nonlinear Wave Processes in Excitable Media*, edited by A. V. Holden, M. Markus, and H. G. Othmer (Plenum Press, London, 1991).
[51] J. R. Weimar, J. J. Tyson, and L. T. Watson, Physica D **55**, 309 (1992).
[52] V. G. Fast and I. G. Efimov, Physica D **49**, 75 (1991).
[53] J. D. Murray, *Mathematical Biology* (Springer-Verlag, New York, 1989).
[54] W. Press, B. Flannery, S. Teukolsky, and W. Vetterling, *Numerical Recipes in C* (Cambridge University Press, New York, 1988).
[55] *Handbook of Mathematical Sciences*, 6th ed. (Chemical Rubber, Boca Raton, 1987).
[56] D. Barkley, Phys. Rev. A **42**, 2489 (1990).
[57] P. Fife, J. Chem. Phys. **64**, 554 (1976).
[58] J. R. Weimar, J. J. Tyson, and L. T. Watson, Physica D **55**, 328 (1992).